1-1-2006

# Asymmetry of Tidal Plume Fronts in an Eastern Boundary Current Regime

David A. Jay
*Portland State University*

Jiayi Pan
*Portland State University*

Philip M. Orton
*Portland State University*

Alexander R. Horner-Devine
*University of Washington - Seattle Campus*



Citation Details

Jay, D. A., Pan, J., P. M. Orton, A. Horner-Devine, 2009, Asymmetry of tidal plume fronts in an eastern boundary current regime, J. Mar. Sys. 78, 442-459.

# Asymmetry of Tidal Plume Fronts in an Eastern Boundary Current Regime

David A. Jay[a], Jiayi Pan[b], Philip M. Orton[c], Alexander Horner-Devine[d]

a. Department of Civil and Environmental Engineering
Portland State University
PO Box 751
Portland, OR 97201 USA djay@cecs.pdx.edu
503-725-4247
corresponding author

b. Department of Civil and Environmental Engineering
Portland State University
PO Box 751
Portland, OR 97201 USA panj@cecs.pdx.edu

c. Ocean and Climate Physics
Lamont Doherty Earth Observatory
Columbia University
61 Route 9W
Palisades, NY 10964 USA orton@ldeo.columbia.edu

d. Department of Civil and Environmental Engineering
University of Washington
Box 352700
Seattle, WA 98195-2700 USA arhd@u.washington.edu

Submitted to Journal of Marine Systems 8 October 2006

**Abstract**

The Columbia River tidal plume or near-field is formed twice daily by the ebb outflow of the Columbia River. It is a part of a larger, anticyclonic plume bulge, which in turn is embedded in far-field plume and coastal waters. Because of the mixing caused directly and indirectly by plume fronts, the interaction of the tidal plume and bulge with the California Current upwelling regime plays a vital role in coastal productivity on the Oregon and Washington shelves. The tidal plume is initially supercritical with respect to the internal Froude number on all stronger ebbs. It is separated from the plume bulge by a front, whose properties are very different under upwelling vs. downwelling conditions. Under summer upwelling conditions, this front is sharp and narrow (only 50-100 m wide on its upwind or northern side) and marks a transition from supercritical to subcritical flow for 6-12 hours after high water. This sharp front is a source of turbulent mixing, despite the strong stratification. Because the tidal plume may overlie newly upwelled waters, these fronts can mix nutrients into the plume, enhancing primary productivity. Symmetry would suggest that there should be a sharp front south of the estuary mouth under summer downwelling conditions. Instead, the downwelling tidal plume front is usually broad (up to several km) and diffuse on the upstream side. Less mixing occurs, and the water immediately below the plume consists of old plume and surface ocean waters, both low in nutrients. There is also a second upwelling-downwelling asymmetry. Supercritical upwelling plume fronts often generate solitons trains as they slow and transition to a subcritical state. These soliton trains contribute to vertical mixing in the plume bulge and have a non-zero Stokes drift so that they transport low-salinity water across the tidal plume into the plume bulge. Under downwelling conditions, soliton formation is uncommon. Moreover, solition formation almost always begins on the south side of the plume so that the front "unzips" from south to north. This implies that a frontal transition from supercritical to subcritical conditions first occurs on the south side tidal plume, regardless of whether this is the upwind or downwind side of the plume.

This contribution describes and analyzes these two asymmetries using vessel data, SAR images and a vorticity analysis. Internal Froude number and plume depth are key parameters in distinguishing the upwelling and downwelling situations, and the observed asymmetries can be explained in terms of potential vorticity conservation. The tidal outflow embeds relative vorticity in the emerging tidal plume water mass. This vorticity controls the transition of the tidal plume

front to a subcritical state and the timing and location of internal wave generation by plume fronts.

*Keywords*: Plumes, Fronts, Solitons, Tidal effects, Eastern boundary currents, Upwelling

## 1. Introduction: Scope and Setting

### 1.1. Scope

A buoyant river plume and its fronts can interact strongly with ambient alongshore flow, influencing thereby vertical mixing, the nutrient supply to coastal waters, and the transport of particles and organisms. This issue has been studied to date in several contexts (e.g., Chao, 1988; O'Donnell et al., 1998; Fong et al., 1997; Hickey et al., 2005; Garcia-Berdeal et al., 2002). It is of particular importance for Eastern Boundary current plumes, because upwelling regimes like the California Current support high levels of primary production and major fisheries (Landry et al., 1989).

This paper documents and interprets the interaction of the Columbia River tidal plume and its fronts with the California Current upwelling/downwelling regime. The "tidal plume" is the water from the most recent ebb. This usage reflects the fact that, for all presently observed river flow levels, outflow from the Columbia River occurs as distinct ebb pulses separated by periods of landward currents through the plume lift-off zone. The tidal plume and its interaction with the upwelling regime are of particular interest, because ~30-50% of the total mixing between river and ocean water occurs in the tidal plume, within about 12 hours after water leaves the entrance area (Orton and Jay, 2005), and fronts play a strong role in this mixing (Nash and Moum, 2005). The results presented below employ both remote sensing data (synthetic aperture radar or SAR and ocean color) and vessel data collected 2004-2006 by the RISE (River-Influences on Shelf Ecosystems) project, funded by the U.S. National Science Foundation (NSF).

Discussion of the interaction of the inner plume with the upwelling regime is conveniently framed in terms of the two asymmetries between tidal plume fronts observed during upwelling vs. downwelling periods. During summer upwelling periods, tidal plume fronts remain supercritical long after they leave the estuary entrance, particularly on their upwind, northern side. They are sharp and narrow (50-100 m wide) and mark a transition from supercritical to subcritical flow for 6-12 hrs after high water. Despite high stratification, these fronts and the internal waves they generate represent a source of vigorous turbulent mixing north of the estuary mouth.

Symmetry would suggest that, under summer downwelling conditions, there should be a sharp front south (upwind) of the estuary mouth. In fact, downwelling tidal plume fronts are usu-

ally broad and diffuse even on their upstream side, because a transition from supercritical to subcritical conditions has already occurred close to the estuary mouth. Much less mixing is accomplished, and the water immediately below the plume consists of old plume and surface waters, both low in nutrients.

There is also a second upwelling-downwelling asymmetry. Supercritical plume fronts often generate multiple solitons as they transition to a subcritical state. These solitons trains contribute to vertical mixing in the plume bulge and have a non-zero Stokes drift such that they transport low-salinity water across the tidal plume into the plume bulge. SAR images show that soliton formation occurs frequently under upwelling or neutral conditions, and infrequently under downwelling conditions. Moreover, solition formation almost always begins on the south side of the plume so that the front "unzips" from south to north. This implies that a frontal transition from supercritical to subcritical conditions first occurs south of the estuary mouth, regardless of whether this is the upwind or downwind side of the plume. We show that these asymmetries can be explained in terms of vorticity conservation.

### 1.2 Regional Context

The Columbia is the fourth largest river in North America, with an average flow of ~7,300 $m^3s^{-1}$. Discharge varies between 2,500 (fall) and 12,500 $m^3\ s^{-1}$ (spring) over a typical year, but reaches 25,000 $m^3\ s^{-1}$ in major winter floods (Bottom et al., 2005). It provides the single largest freshwater inflow along the Pacific Coast of North and South America. Thus, the Columbia plume is a dominant feature in the hydrography of the Oregon and Washington coasts, sometimes transporting particles, organisms, and contaminants hundreds of kilometers along and across the continental margin (Barnes et al., 1972, Thomas and Weatherbee, 2005, and Fig. 1). The highest regional rates of primary productivity and standing stock of chlorophyll are associated with regions influenced by freshwater in spring; i.e., the plume itself and the Washington shelf. These areas are also vital to the survival of juvenile salmonids, several races of which are classified as endangered (Casillas, 1999). The spring and summer spatial extent of the plume has been greatly reduced by reduction of spring freshet volume by >40% due to flow regulation and irrigation diversion.

**Figure 1**

Broadly speaking, the Columbia plume flows northward over the shelf during fall and winter downwelling periods, and southward offshore of the shelf during spring and summer upwelling (Figs. 2-4), but these canonical configurations can occur any time of year, because the plume changes direction, thickness and width in response to frequent local wind stress fluctuations (Hickey et al., 1998, Garcia-Berdeal et al., 2002). Periods of variable winds, especially frequent in May and June, result in a "bi-directional" plume with freshwater north and south of the river mouth (Hickey et al., 2005). Because of the weak barotropic tidal currents and the high buoyancy input, the Columbia Plume near-field and bulge are very stratified, with the 3-10 m thick plume overlying shelf waters. Unlike the more-studied Rhine plume with a lower buoyancy input and stronger tides (e.g., Souza and Simpson, 1997), mixing extends to the bed only beneath the tidal plume front. In the parlance of Yankovsky and Chapman (1997), the Columbia plume is in the "surface-advected" category, due to the relatively narrow, steep shelf off the river mouth.

There are several reasons why the Columbia plume is itself highly productive and contributes to regional primary production:

- The paradoxical nature of plume mixing: Despite high stratification, plume fronts exhibit vigorous mixing and disturb the seabed down to at least 50-60 m (Orton and Jay, 2005), mixing upwelled nutrients and iron (Fe) from re-suspended river sediments into the surface layer.
- Plume micronutrients: The plume supplies iron (Fe) and manganese from land (Jay et al., 2002; Lohan and Bruland, 2006).
- Compensating production: Elevated riverine nutrient input to the plume productivity due to precipitation over the coastal subbasin of the Columbia River partially compensates for primary production lost during periods of prolonged downwelling. This mechanism is most important during years like 2005 when strong upwelling is delayed (cf. Fig. 2).

**Figures 2, 3 and 4**

An important feature of the Pacific Northwest coastal ecosystem is that the standing stock of chlorophyll and primary productivity are both higher on the Washington shelf than the Oregon shelf (Landry et al., 1989; Hickey, 1989). The fact that the movement of plume water is often northward and onshore in a coastal current during downwelling vs. offshelf and southward dur-

ing upwelling is one factor that may explain this observation. The northward movement of Fe-rich silt during winter storms is another important factor. We suggest in Section 5 that differences between upwelling and downwelling tidal plume fronts are also important. Upwelling fronts exhibit stronger mixing, and are more likely to mix plume and recently upwelled waters; this mixing occurs primarily north of the estuary mouth. Thus, frontal propagation provides a mechanism for mixing on the shelf and slope in the sense of Kelvin wave propagation relative to the estuary mouth, where it would otherwise be suppressed by the stratification of the plume.

## 2. Plume Anatomy and Frontal Dynamics

### 2.1. Plume Structure and Function

The Columbia River tidal plume overrides and interacts with a larger anticyclonic plume bulge, which in turn is embedded in older plume and coastal waters. Understanding plume processes requires terminology for plume functional components. Garvine (1982) divided a steady buoyant plume into three zones or regimes: a source zone, the near-field and the far-field. The strongly tidal Columbia plume requires, however, distinguishing between the tidal plume and the plume near-field (Fig. 5). Thus, the plume components are:

- The Plume Source Zone: The plume source zone is the area at the entrance of the estuary where low-salinity estuarine waters lift-off from the seabed to form the nascent plume.
- The Tidal Plume: The tidal plume or near-field consists of the most recent ebb outflow from the plume and is surrounded by strong fronts. It remains distinct from the plume bulge until its fronts become subcritical, at which time it merges into the bulge. The scaling of the tidal-plume and plume bulge is considered in Horner-Devine et al. (2007, this volume).
- The Plume Bulge: The bulge extends seaward from the tidal plume. It usually contains the water from several ebbs and is separated from the plume far-field by a diffuse frontal zone, sometimes visible in remotely sensed images.
- The Plume Far-Field: The far-field is the zone beyond the bulge where final mixing of plume and ambient seawater occurs; S = 32 to 32.5 defines its outer boundary (Barnes et al., 1972).

These zones provide a good basis for a more detailed description of the specific features of Columbia tidal plume fronts.

**Figure 5**, from Horner-Devine et al., this volume

2.2 Plume Fronts, Vorticity Constraints and Internal Froude Number

Analysis of tidal plume vorticity conservation is useful because it illuminates tidal plume behavior. We are also interested in the implications of vorticity conservation for the internal Froude number ($F_R = U_f/(g'H)^{1/2}$; $U_f$ is frontal speed) associated with the tidal plume front, because $F_R$ governs plume frontal behavior. Consider conservation of potential vorticity $\Omega = (f + \xi)/H$ following a parcel of water in inviscid motion. [Here $\xi = (\partial v/\partial x - \partial u/\partial y)$ is the vertical component of vorticity, and $H$ and is plume depth]. As described in the following paragraphs, the tidal stream (the ebb jet) at the estuary entrance and alongshore coastal currents transfer their vorticity to the nascent plume, increasing plume velocity, considerably altering its vorticity dynamics, and changing the time and space variations of $H$.

Assume for purposes of this argument that the plume is inviscid but that it takes on vorticity from the underlying tidal and coastal flows. Conservation of $\Omega$ and mass following an emerging parcel of plume water assumed to be at or near the plume front in the center of the emerging plume requires:

$$\frac{1}{(f+\xi)}\frac{D(f+\xi)}{Dt} = \frac{1}{H}\frac{DH}{Dt} \;\Rightarrow\; \frac{D\frac{(f+\xi)}{H}}{Dt} = \frac{D\Omega}{Dt} = 0 \qquad (2.1)$$

$$\nabla_H \cdot \mathsf{U}_H = -\frac{1}{H}\frac{DH}{Dt} \qquad (2.2)$$

Where: $\mathsf{U}_H = \{u,v\}$ is the plume horizontal velocity, and $\nabla_H = \{\partial/\partial x, \partial/\partial y\}$; $x$ is onshore and $y$ to the north. The initial mid-channel condition as the front emerges is that $\xi = 0$ because: a) $v = \partial v/\partial x \sim 0$ (the flow is straight west and axially non-divergent in a channel of nearly constant width and depth), and b) $\partial u/\partial y = 0$ in mid-outflow because the tidal outflow is strongest in mid-channel. There is, however, lateral shear in ebb currents which confers vorticity on the tidal out-

flow as a whole, as does the lateral spread of the jet-like ebb outflow (Chao, 1990). Specifically, $\partial v/\partial x < 0$ and $\partial u/\partial y > 0$ north of the channel centerline, while $\partial v/\partial x > 0$ and $\partial u/\partial y < 0$ south of the channel centerline.

Now consider fronts on the upwind side of the river mouth for first upwelling and then downwelling conditions (Figs. 6a,b):

- Upwelling: the winds are from north to south, and the upwind front is to the north of the river mouth. It remains supercritical (with respect to $F_R$) for 6-12 hrs after high water, with a very sharp front (Orton and Jay, 2005, Section 4). For water in a northward turning plume front, the spreading and rotation of the tidal outflow causes $\xi$ to decrease; $\xi$ is < 0, and the rotation is anticyclonic (Fig. 6a). The rapid motions associated with the initial tidal outflow (up to 3 $ms^{-1}$) cause changes in $f$ to be small relative to those in $\xi$. Therefore, $H$ must decrease to conserve $\Omega$, making the plume near the front shallow and fast, from (2.1). From (2.2), the plume spreading necessary to decrease $H$ can occur both by axial and lateral divergence. Given any fixed density contrast, the small $H$ and high velocity will raise the frontal internal Froude number $F_R$. The front stays sharp, because waves cannot propagate away from it. Frontal energy is eventually lost by a pulse of soliton generation, but this typically occurs after the end of ebb, well into the following flood.

  The coastal flow contributes to frontal convergence, and more strongly during upwelling than downwelling, because the oncoming flow for upwelling conditions is typically larger during the summer season considered here – the coastal jet may reach 0.5 $ms^{-1}$ at the surface; see Section 4.1. The combination of strong anticyclonic movement in the plume and the fact that the coastal flow turns to some extend away from the coast to go around the plume means that there is strong shear along the front, as well as strong convergence. Because the plume front remains supercritical for so long, we expect it to move farther upwind (north) against the ambient flow than would be the case during downwelling, despite the opposition of a stronger coastal current.

  The vertical density contrast between plume waters and the underlying flow also affects $F_R$ in a different way during upwelling vs. downwelling. Upwelling pushes old plume water away from the coast, replacing it by high salinity ($S$), low temperature ($T$) upwelled water, yielding

a high value of $g'$. This initially high value of $g'$ does not, however, preclude supercritical conditions from occurring at the plume front, because variations in $U_f$ and $H$ are dominant. Moreover, strong mixing disproportionately reduces $g'$ during upwelling vs. downwelling, helping to maintain $F_R > 1$.

**Figure 6**

- Downwelling: the winds are from south to north, and the upwind front is to the south of the river mouth (Fig. 6b). The upwind front is subcritical ($F_R < 1$) soon after it leaves the source zone, with a broad, diffuse front. For the waters in a southward turning plume front, the spreading and rotation of the ebb jet cause $\xi$ to increase such that $\xi > 0$, and the sense of rotation is cyclonic. Since changes in $f$ are small relative to those in $\xi$, $H$ must increase, slowing and deepening the plume, from (2.1). From (2.2), lateral spread (plume divergence) must be compensated by strong axial convergence to satisfy (2.1) and increase $H$. Given any fixed density contrast, low frontal velocity and high $H$ will both lead to a low value of $F_R$, even if the initial density contrast is less than in the upwelling case. The front is diffuse, because the front is sub-critical and energy can propagate away from it. During summer, northward flow during downwelling is usually weaker than the coastal jet during upwelling. Because the plume front becomes subcritical shortly close to the mouth, its movement upwind (south) is usually less than during upwelling, despite a relatively weak coastal current. These travel distances are, however, also affected by tidal range – fronts spawned on spring tides travel farther than on neap tides.

  Downwelling traps old plume water near the coast, reducing the initial $g'$, but not usually enough to allow the plume front to be supercritical ($F_R > 1$) for very long. Whatever the initial density contrast, it is not greatly altered by mixing, because shears are lower than during upwelling.

The above discussion assumes that $\xi$ is not affected by vertical mixing. Mixing, which is stronger during upwelling than downwelling, alters frontal propagation, e.g., by limiting the speed of the northward moving upwelling front. Still, the above inviscid vorticity analysis explains important bulk plume properties. Thus, a north-south section across the plume shows that it is indeed deeper on the south side, with weaker currents (Fig. 7). Fig. 7 was taken during a

weak ebb under moderate river flow and tide conditions. The low salinity water seen at the north end of the section remains from the previous ebb pulse, and is no longer supercritical. The anti-cyclonic rotation (negative vorticity) of the plume, characteristic of its mean circulation (Hickey et al., 1998) is evident. Nonetheless, the low salinity waters south of the estuary mouth must have initially obtained positive vorticity during the previous ebb outflow to reach a position south of the river mouth, and the north-south slope of the pycnocline is related to the initial tidal vorticity distribution. The observations of the Connecticut River plume by O'Donnell et al. (1998) show a similar decrease in plume depth for waters with a more negative vorticity (judged by their position). Because the Connecticut plume always turns left with the ebb in Long Island Sound, it is not possible to compare upwelling plume and downwelling plumes for that system.

**Figure 7** from Horner-Devine et al. (2007, this volume).

## 3. Methods: Data collection and Processing

### 3.1 Vessel Data

RISE physical oceanography was carried aboard *R/V Pt Sur*. Sampling the plume is quite challenging, because the plume is shallow (2-10 m) and highly mobile. It varies on time scales of less than a day and is characterized by relatively large length scales that are difficult to cover synoptically with a single vessel (Hickey et al., 1998). Therefore, both vessel and remote sensing data are used herein. *R/V Pt Sur* carried out rapid surveys using a towed body (the TRIAXUS, steerable in 3D) and the vessel's near-surface underway data acquisition system or UDAS (nominally at 3 m depth). The high mobility of TRIAXUS was used to sample surface waters (up to within 0.5-2 m of the surface, depending on sea state) outside of the ship wake. Three cruises were conducted during which TRIAXUS data were collected. RISE1 (July 2004) occurred during a period decreasing river flow after a weak spring freshet; prolonged upwelling was seen at the end of the cruise. RISE2 (June 2005) occurred during decreasing river flow after a weak spring freshet; strong upwelling was absent. RISE4 (June 2006) had moderately high but decreasing river flow; some weak upwelling was observed.

The *R/V Pt Sur* carried a pole-mounted acoustic Doppler current profiler or ADCP [300 kHz in 2004 (RISE1) and 1200 kHz in 2005 and 2006 (RISE2 and RISE4)]. The *R/V Pt Sur* UDAS

acquired position, meteorological data, salinity (S), temperature (T), and fluorescence at 3 m. TRIAXUS carried a 911 SeaBird conductivity-temperature-depth (CTD) profiler equipped with sensors for nitrate (N), C, T, pressure, transmissivity and fluorescence and two Ocean Sensors fast-response OS-200 CTDs to measure density fine structure. CTD casts were made at the beginning and end of maps with a second, identical SeaBird 911 CTD for calibration purposes. The vessel and pole-mounted ADCP data sets are used in the analyses described herein, along with scalar data from TRIAXUS.

### 3.2 Remotely Sensed Data

Synthetic aperture radar (SAR) and ocean color images are used in this study to provide synoptic coverage of the plume area. SAR images were obtained from RADARSAT-1, launched in 1995. The SAR raw data were processed at the Alaska Satellite Facility, Fairbanks, Ak. The processed SAR images are archived and distributed through the Comprehensive Large Array-data Stewardship System (CLASS) of National Oceanic and Atmospheric Administration (NOAA). Here, our use of the images involves rectification and editing to include only the relevant region near the mouth of the Columbia.

The ocean color data used here are from the Moderate Resolution Imaging Spectroradiometer (MODIS) aboard an Aqua satellite, launched on 4 May 2002. Aqua MODIS views the entire Earth's surface every 1 to 2 days, acquiring data in 36 spectral bands. The MODIS ocean color data have been processed using O'Reilly et al. (2000a) for chlorophyll a (Chl-a) and Van Mol and Ruddick (2005) for suspended particulate matter (SPM). To obtain concentrations of Chl *a* and suspended particulate matter (SPM), we used the normalized water leaving radiance (nLw) at bands of 412 nm, 443nm, 488nm, 531nm, and 551nm. The nLw data are available from: http://oceancolor.gsfc.nasa.gov.

### 3.3 Turbulence Estimates from Fine Structure

Quantifying vertical turbulent near plume fronts is an important part of understanding the role of these fronts in the Columbia plume ecosystem. We have estimated turbulence parameters from the fine structure observed by TRIAXUS CTDs through a fine-structure, turbulent length-scale analysis. This method is applicable to stratified areas with at least moderately strong mix-

ing. TRIAXUS was towed in a "tow-yo" saw tooth pattern, with horizontal and vertical speeds through water of ~3 m $s^{-1}$ and ~1 m $s^{-1}$ respectively. The SBE-911 sampling rate was 24 Hz, and the OS200 sampling rate was 9 Hz, though the actual sensor response times for the two types of instruments are similar. The OS200 was successfully used for detecting density fine-structure overturns by Orton and Jay (2005). Here, we present SBE-911 results, because the SBE-911 has a lower noise level, and the stratification is weaker than in our previous study. As expected from their relative noise levels, the OS200's usually detected the same overturns as the SBE-911 when they involved overturn sizes above the OS200's noise floor.

The statistics arising from a Thorpe sort are used to estimate turbulence parameters. A Thorpe sort restores each measured density vertical profile to a monotonic form representative of its mean (Thorpe, 1977). The sorting density yields a profile of $L$, the vertical distance over which each gravitationally unstable density data point has been moved. The Thorpe scale $L_T$ is the rms of $L$ in each overturn patch, a patch defined as a unstable region where the values of L sum to zero (Seim and Gregg, 1994). Strict quality control methods are used to avoid spurious overturns from measurement noise and from the horizontal movement of the towed platform (Galbraith and Kelley, 1996; Ott et al., 2004; Orton and Jay, 2005). Over-turns with rms density inversions less than the resolution of the sensor are eliminated, as are areas near fronts with strong isopycnal slopes.

Dissipation of turbulent kinetic energy ε is estimated (Thorpe, 1977):

$$\varepsilon = a^2 \overline{L_t^2 \langle N^3 \rangle} \qquad (3.1)$$

Here, angle brackets denote an average over an overturning patch and the overbar an average over several profiles; $N$ is the buoyancy frequency and $a \approx 1$. Eddy diffusivity $K_\rho$ is (Peters and Johns, 2004):

$$K_\rho = a^2 \Gamma \overline{\langle N \rangle L_T^2} \qquad (3.2)$$

Here, the mixing efficiency is approximated as $\Gamma \approx 0.22$ for coastal stratified flows (Kay and Jay, 2003; Macdonald and Geyer, 2004).

Mixing estimates are presented as transect-averages, referenced to depth and density surfaces, with conservative floor and ceiling estimates. The floor is derived from averaging all data,

including zeroes where no overturn was observed. The ceiling is derived from averaging all data, but substituting the minimum detectable value wherever no overturn was observed.

## 4. Results: Plume Front Dynamics

### 4.1. Summer Plume Configurations

The tidal plume and plume near-field are embedded within the plume as a whole. The size and position of the bulk plume is related to the amount of river outflow provided by the Columbia, ambient currents, and coastal winds (Fig. 8). There are four plume configurations that occur frequently during spring and summer in response to variable forcing: prolonged strong upwelling (Fig 5c), downwelling (Fig 5a,b), and bi-directional. A typical example of variable summer winds and currents observed at a mooring in the plume area is shown in Fig. 8 for July 2004 (see Fig. 6a for mooring location). Light and variable winds of < 5 $ms^{-1}$ prevailed until 17 July. This was followed by a brief downwelling episode 18-20 July with winds to 6 $ms^{-1}$, then persistent upwelling favorable winds as strong as 7 $ms^{-1}$ on the 21 July; winds thereafter were lighter. While there is only a small disparity in the magnitude of the upwelling vs. downwelling-favorable winds, there is a much stronger difference in the currents at 1.5 m depth. Southward near-surface currents exceed 0.4 $ms^{-1}$ on two occasions, while northward currents never reach 0.2 $ms^{-1}$. This disparity occurs only at the surface – at 25 m, currents are predominantly northward, while depth-averaged currents show little predominance. This mooring in Fig. 8 is most representative of conditions in the plume near-field, but the other two RISE moorings show a similar (or larger) predominance of surface flow to the south.

**Figure 8**

Though there are four common summer plume configurations, we focus here on prolonged upwelling and downwelling, because these two situations capture the frontal processes of interest. A typical plume configuration associated with prolonged upwelling is shown in Figs. 9 and 10. A SAR image of fronts prevailing at that time is shown in Fig. 6a. These data were collected 24-27 July 2004. They reflect a plume configuration established by upwelling-favorable winds that had persisted since late 20 July 2004 (Fig. 8). Columbia River flow at the most seaward gauging station (Beaver, 85 km from the ocean; waterdata.usgs.gov/or/) was 3,600 to 4,400 $m^3s^{-1}$ for 20-27 July 2004; tidal forcing was weak. The 2004 spring freshet was smaller than normal,

and this flow level represents only about 55% of the long-term average of 7,300 $m^3s^{-1}$. Fig. 9 shows the plume moving southward and off the slope with S < 31 water as far south as 45.3º N. Newly upwelled water (S > 33.5) reaches the surface inshore of the new plume south of 46º N. The UDAS Chl-a data (Fig. 9) show productivity along the outer edge of the new plume to the north of the entrance and as its spreads offshore (cf. Fong and Geyer, 2001) between 45.95º N and 46.2º N, and at the inshore end of several lines.

An ocean color-derived Chl-a map for 23 July 2004 suggests strong productivity inshore of the plume, where some mixing of plume and upwelled water has occurred (Fig. 10). There is also some productivity in a band extending offshore through the plume at about 45.85º N. A similar map for 22 July 2004, just after the onset of upwelling, suggests strong productivity around the margins of the plume, especially on its south side. This productivity is likely associated with mixing of upwelled water with the plume as the plume bulge thinned and spread south into an area not occupied by the bulge the previous day. This interpretation is supported by a broad band of T = 12-14º C water on the 22 July 2004 SST map that corresponds to the higher productivity; new tidal plume waters had *T* = 15-17º C at this time. The UDAS Chl-a map in Fig. 9 generally agrees with Fig. 10, but fails to define the band of production extending offshore, likely because this feature was transient.

**Figures 9 and 10**

Salinity and Chl-a for a typical plume configuration associated with downwelling are shown in Figs 3,4. These observations were collected 18-20 June 2005 just before a spring tide and two days after a transition to downwelling favorable winds on 16 June 2004. Winds were weak and variable by the end of the map. River flow averaged 6,400 $m^3s^{-1}$ and was decreasing slowly after the peak of the spring freshet on 20 May 2004 (~10,000 $m^3s^{-1}$). Old plume water from a previous upwelling episode is seen inshore south of the river mouth to 46.05º N. The lowest salinity water associated with the tidal plume water is directly offshore of the mouth at 45.5º N. The ocean color Chl-a map in Fig. 4 shows moderate levels of Chl-a associated with the plume bulge, north of the river mouth, but little Chl-a associated with coastal upwelling.

4.2 Upwelling Frontal Phenomenology and Processes

The observations of upwelling plume fronts used here stem from 13 June 2005, a neap tide. Partial ocean color data for 13 June 2005 (not shown) suggest the large scale picture at that time was similar to that shown in Fig. 2 for 29 May to 3 June 2005. The light northwesterly (upwelling-favorable) winds that began on 12 June 2005 were sufficient, in any event, to cause tidal plume fronts to behave in the manner similar to Fig. 6a. River flow for the week prior to 13 June averaged about 6,800 $m^3s^{-1}$, down from a freshet peak on 20 May 2005 of 10,200 $m^3s^{-1}$, and more than 3,000 $m^3s^{-1}$ below season average for mid-June.

SAR images frequently show solitons propagating seaward from the tidal plume front. Usually they also define a "fission point" – the location at which a soliton is just leaving the plume front (cf. Fig. 6a). As discussed in Section 4.4, the fission point moves from south to north, "unzipping" the front to produce non-linear internal waves or solitons. The TRIAXUS section in Fig. 11 captures the initial fission of a northwestern front, ~5.6 hrs after high water. Fig. 12 shows a detail of a later stage of evolution of the soliton train, starting, 8 hrs after high water.

**Figures 11 and 12**

The front shown in Fig. 11 has moved >15 km in 5.6 hrs. For an upwelling front, this constitutes an early transition to a subcritical state. The early transition is likely due to weak tidal forcing and high ambient stratification, the latter related to the recent high river flow levels. The double depression in Fig. 11 represents the front (to the right at 124.314º W) and the newly spawned soliton left of the front (at 124.318º W). The tidal plume is 6-10 m deep for several km behind the front at the time of fission, as judged by the depth of the S = 22 contour (Fig. 11a). The front, on the northwest side of the tidal plume, is propagating at 0.54 $ms^{-1}$ into a relatively stratified plume bulge (as suggested by Fig. 5c), the surface layer of which is also moving away from the front (Fig. 11b). High S, upwelled waters are found below 25-30 m. The front remains slightly supercritical ($F_R$ = 1.04) in Fig. 11, despite release of a soliton.

At the front, there is a surface salinity difference S >10 between successive TRIAXUS passes, ~200 m apart (Fig. 11a). The acoustic section (Figs. 11c,d) suggests that the actual frontal width (judged by the width of the plunge) is ~60 m, which accords with visual observations and

ship radar images. O'Donnell et al. (2006) argue that, from laboratory experiments, the width of coherent structures at the plume front should be $L_F = 5\ \Delta U/N$, where: $\Delta U$ is the velocity difference between the plume layer and the underlying flow, and $N$ is the buoyancy frequency. Based on this scaling, we expect a plunge width $L_F$ = ~20 m, smaller than the observed plunge width by a factor of three. When O'Donnell et al. applied this estimate to the Connecticut plume, they found $L_F$ to be too small by a factor of 1.5-2. A variety of factors may contribute to the discrepancy, including interaction with internal waves and 3-D frontal circulation.

CTD, velocity and acoustic data show that the plume front is very energetic, despite the weak tidal forcing and prior release of a soliton (Fig. 11). In terms of vertical motion, the plunge at the plume front affects the density field down to ~25 m. The first soliton is even more energetic, penetrating to the bottom of the section at 33 m. Thus, despite the high stratification of the plume bulge area, plume fronts and the solitons generated from them can cause mixing down to the level of high S, upwelled water.

Release of a soliton train greatly alters frontal structure. The frontal crossing shown in Fig. 12 occurred about 3 hrs after (at ~2100 UT) after that in Fig. 11. The plume front is much broader (~2 km), has lost energy to the soliton train, and has slowed to 0.13 $ms^{-1}$, with $F_R = 0.18$. The tidal plume has also shoaled with the S = 22 contour at 6-8 m (Fig. 12a), while the pycnocline seaward of the front has deepened to a mean depth of ~12-13 m. There are four large solitons between the front at 124.37º W and 124.45º W (Fig. 12a-c). The deepening of the pycnocline seaward of the front has apparently occurred through the advection of plume waters seaward via a Stokes drift mechanism (Pan and Jay, 2006a,b). The phase speed of such solitons is O(0.5-1 $ms^{-1}$), similar to the frontal speed at $F_R = 1$. The lead soliton can, therefore, move 5-10 km away from the front in the three hours between the frontal crossings in Figs. 11 and 12, consistent with the position of these waves in Fig. 12. On stronger tides, more solitons are released; e.g., 10-12 solitons are visible in Fig. 6a, and a ship radar image for 8 June 2005 showed 15.

Fig. 13 shows turbulence parameters for the transect of Fig. 11. Overturns occur landward of the front, presumably in the front itself (where a fine-structure method cannot document them), and to a lesser extent seward of the front. Pan and Jay (2006a) have argued that the internal wave shear plays a crucial role in augmenting to mean shear in this area, allowing mixing to occur

where it would not be possible on the basis of mean shear alone. The sectionally averaged scalar diffusivity $K_\rho$ (up to $>10^{-3}$ $m^2s^{-1}$) and dissipation (up to $3\times10^{-1}$ W $m^{-3}$) for waters with density anomaly $\sigma_T < 18$ are quite high. Lower values pertain for higher salinity waters, especially those outside the plume (Fig. 13c). Because the fine-structure method used here does not allow mixing estimates in the front and in some profiles through the internal waves, Fig. 13 is a conservative estimate of plume mixing. Still, Figs. 11 and 13 confirm that tidal plume fronts influence the density field down to 25-30 m, as in Orton and Jay (2005).

**Figure 13**

In summary, tidal plume fronts during summer upwelling conditions typically:

- Remain supercritical ($F_R > 1$) for 6 to 12 hrs after high water, travelling 15-25 km from the river mouth before becoming subcritical.
- Are very sharp on the upwind (north) side of the river mouth, with widths ~50 m.
- Are shallower on the upwind side of the plume than downwelling fronts, and accomplish more mixing.
- Are underlain by surface ocean water and upwelled water, the later of which is high in nutrients (N and P). Thus, they should contribute to primary production more effectively than downwelling fronts.
- Spawn, upon transition to subcritical conditions, an energetic soliton train that contributes to mixing outside the plume and carries tidal plume water across the front.

These properties are consistent with vorticity analysis for upwelling conditions (Section 2.2) – conservation of potential vorticity requires that frontal waters on the upwind (north) side of the river mouth (which have negative relative vorticity from the tidal outflow) must diverge and accelerate. This thins the plume, maintains the front in a supercritical state and increases mixing associated with the upwelling fronts. During summer at least, southward alongshore flow during upwelling periods is relatively strong, and shear between the plume and the underlying coastal flow contributes to keeping the tidal plume supercritical for a long period. These fronts often spawn solitons even in winter (when southward flow is weak or absent), suggesting that the change in vorticity associated with the turn of the tidal flow to the north from the estuary mouth

(not alongshore flow) is the dominant factor controlling their behavior and differentiating them from downwelling fronts.

4.3 Downwelling Frontal Phenomenology and Processes

The observations used to describe typical summer downwelling frontal phenomena stem from 19 July 2004; a regional salinity map is shown in Fig. 3. This downwelling episode was brief (17-20 July), with peak poleward winds on 18 July of ~6 $ms^{-1}$. Fig. 14 shows a SAR image for 19 July 2004 at 1428 UT, 2 d after a spring tide. Superimposed on the SAR image are two 3 m salinity traces (from the *R/V Pt Sur* UDAS) across the frontal zone, covering the time period from 1322 to 1511 UT, ~4 to 6 hrs after high water. While a moderately sharp front is seen at ~46.17º N in the earlier of the two transects, the second crossing of the frontal zone (corresponding to the time of the SAR image) shows a diffuse frontal zone at ~46.2º N. Thus, the SAR image and surface salinity trace suggest the possibility of a transition from supercritical to subcritical conditions between the times of the two transects. No solitons were generated in the southern sector by this front, but there may have been a single soliton released on the west side of the plume, between 46.23 and 46.3º N. As suggested by Fig. 5a,b, soliton release on the west but not the south side of the plume may be related to greater stratification directly offshore from the mouth. Lower frontal energy levels on the south side of the plume are also likely involved. Finally, there is, just inshore of the one plume-front soliton in Fig. 14, a train of landward-propagating internal waves. It is also possible that interaction between this wave train and the front influenced the release of the soliton in Fig. 14.

The TRIAXUS sections corresponding to the surface traces in Fig. 14 are shown in Figs. 15 and 16. The first section, the more landward of the two in Fig. 14, shows a well-defined front, ~300 m wide as judged from the salinity transition zone (Fig. 15a). The front is propagating at 0.59 $ms^{-1}$ into nearly motionless (Fig 15b), weakly unstratified water (cf. Fig. 5a,b). Total propagation distance over 4.5 hrs is ~15 km. There is a plunge defined by a single ADCP ensemble, which penetrates >30 m, deep enough to cause some mixing with high S, upwelled waters. The front is supercritical, with $F_R$ = 1.86. Between the two sections, the plume deepened and became just subcritical (Fr = 0.93); its front is more diffuse. Also, the base of the plume (judged by the S =31 contour) is at 8-14 m at right, deeper than in the upwelling case (compare Figs. 11-12 with

Fig. 16). After the transition to subcritical, the frontal speed has slowed to 0.14 $ms^{-1}$. The frontal plunge is barely visible in the ADCP record (Fig. 16b), affecting the flow only to about 12 m. Even though this is a spring tide and the sections were occupied before the end of the ebb (4-6 hrs after high water), the frontal zone is ~2 km wide (from ~46.167 to 46.2º N). The two deeper areas behind the front (centered at ~46.2º N and 46.25º N) apparently correspond to the two broad features on the SAR image (Fig. 14).

Clearly, this downwelling front is more diffuse than the upwelling front in Figs. 11-13. It is also less energetic. Mixing estimates from fine structure (not shown) for the transects in Figs. 15 and 16 indicate much less mixing than for upwelling; maximum $K_\rho$ and $\epsilon$ values are both lower by a factor of ~3 to 5, despite lower stratification in the downwelling case. This situation is typical for downwelling conditions – upwind fronts during downwelling make an early transition to subcritical, usually without releasing solitons. The absence of solitons may be related to the low ambient stratification as well as to lower frontal energy levels. What is unusual about this pair of sections is that we were able to capture supercritical condition at all. Normally the transition to subcritical conditions occurs close to the estuary mouth, in an area too shallow for TRIAXUS observations. It is likely that an atypically long period of supercritical propagation occurred because of the large tidal range prevailing at this time.

**Figures 14, 15 and 16**

In summary, tidal plume fronts during summer downwelling conditions typically:

- Make an early transition to a subcritical state, <5-15 km from the estuary mouth and before the end of ebb.
- Are, after transition, diffuse on the upwind (south) side, with widths of 0.5-7 km, such that "frontal zone" is perhaps a better descriptor than "front".
- Are deeper on the upwind side than upwelling fronts, and accomplish less mixing.
- Usually do not spawn soliton trains that contribute to mixing outside the plume.

These properties are consistent with vorticity analysis for downwelling conditions (Section 2.2) – conservation of potential vorticity requires that frontal waters on the upwind (south) side of the river mouth that acquire positive vorticity from the tidal flow must converge axially

and decrease in speed, delaying the thinning of the plume. This causes an early transition from supercritical to subcritical conditions and reduces the mixing associated with downwelling plume fronts. During summer at least, northward alongshore flow during downwelling periods is relatively weak, and is unable to keep the tidal plume supercritical. SAR images suggest that stronger winter northward flows do sometimes cause the upwind, downwelling front to remain supercritical, but internal wave generation is still unusual for upwelling plume fronts. This again suggests that the vorticity of the ebb outflow, not differences in alongshore flow, is the dominant reason for the asymmetry of upwelling vs. downwelling tidal plume fronts.

### 4.4 Asymmetry of Internal Wave Generation

Sections 4.2 and 4.3 document the differences in frontal properties between upwelling and downwelling plume configurations. This section focuses on differences in internal wave generation. A total of 55 images for the 2001-2004 period are available for upwelling (winds predominantly to the south) conditions, and 43 for neutral (winds not predominantly alongshore) conditions. Internal waves generated at the plume front are visible in ~25% of the neutral and upwelling cases. In every case showing internal wave generation from upwelling or neutral conditions, the front "unzips" from south to north, in accordance with the vorticity conservation arguments in Section 2.2. This is true even in situations where the tidal plume departs substantially from its usual circular pattern, e.g., Fig. 17 taken 9 August 2002 under upwelling conditions, about 6.5 hrs after high water on a spring tide. Despite a strong ebb, there has been a relatively early transition from supercritical to subcritical conditions. The tidal plume has two distinct lobes, one to the north and one to the south. Each has generated solitons, unzipping from south to north. Judging from the soliton propagation distance, the southerly lobe was the first to become subcritical, consistent with expectations from vorticity conservation arguments. Also, the southern lobe appears to have generated two sets of solitons. Additionally, shoreward-propagating internal waves are seen along the coast south of the river mouth and southwest of the tidal plume; these may have influenced frontal soliton generation.

Generation of soliton trains by downwelling plume fronts is, in contrast to upwelling plume fronts, uncommon. In those few cases where soliton generation has been observed, it usually proceeds south to north, just as for upwelling. Fig. 15 provides one example of this phenomenon

– careful examination at high magnification shows that generation has proceeded from south to north. Fig. 18 shows a SAR image for a more energetic case. The image was acquired 26 May 2002, ~6 hrs after high water (greater ebb, spring tide); the river flow over the previous week fluctuated from ~6,800 and 8,700 $m^3s^{-1}$. As expected for the upwind front under downwelling conditions, the front on the southerly side of the tidal plume has become indistinct by the end of ebb, despite the strong currents associated with a spring tide. The tidal plume front has unzipped from the southern quadrant to the northwest side, and an internal wave train is seen along the entire west side of the tidal plume.

**Figures 17 and 18**

In summary, almost all images of internal wave generation from tidal plume fronts show that the front first became subcritical on the south or southwestern side of the tidal plume, leading to "unzipping" of the front from south to north. The most likely explanation of this behavior is that vorticity embedded in the emerging plume by the tidal outflow, not the strength and direction of alongshore currents, primarily controls the timing and location of internal wave generation from fronts.

## 5. Discussion and Conclusions

### 5.1. Tidal Plume Fronts and Internal Wave Generation

Tidal plume fronts play a vital role in mixing of plume waters into the bulk plume, and in nutrient supply to the plume. Strong mixing occurs much of the way around the periphery of the tidal plume, presumably anywhere the plume is supercritical (Orton and Jay, 2005). Mixing occurs in association with frontal passage and, after soliton release, due to the combination of mean and internal wave (soliton) shear (Pan and Jay, 2006a). Soliton generation is common during upwelling and neutral periods with cross-shore winds, but much less common during downwelling periods.

The Nash and Moum (2005) and Orton and Jay (2005) analyses and the results discussed here suggest that, for solitons to form, a front must be initially super-critical, with strong frontal convergence causing formation of a bore head. A sub-critical front with a small bore-head will lack the energy to release solitons. The stratification of the ambient ocean outside the plume

front is also vital, however, and this is one reason that the plume region is so rich in solitons. The ocean on the seaward side of the front must be stratified (but not too stratified) such that the soliton propagation speed is less than the initial plume propagation speed, but greater than the intrinsic (linear wave) propagation speed of the stratified coastal ocean. Furthermore, soliton formation modulates the strength and propagation of fronts. The strongest fronts on the north side of the front during upwelling conditions maintain rapid propagation for up to 12 hrs past high water. They often spawn solitons, but may not where they propagate into nearly unstratified, high-salinity upwelled water. The resulting solitons both transport freshwater across the initial plume front and propagate energy that may cause mixing outside the immediate plume bulge. Thus, plume fronts and solitons play an important role in plume and regional productivity.

### 5.2. Tidal Plume Fronts and Coastal Primary Production

Section 4 suggests that frontal processes and solitons drive strong mixing that contributes to high productivity around the margins of the plume near-field. The mixing and its impact on productivity are strongest on the west and northwest sides of the plume (and sometimes also the north side), because:

- The vorticity transferred to the tidal plume by the ebb outflow makes these fronts very energetic, causing the most mixing within the tidal plume and releasing the most energy in the form of solitons to facilitate mixing within the rest of the plume bulge.
- Strongly supercritical fronts occur preferentially during upwelling conditions when nutrients N and P are available from upwelled water to be mixed with plume Si and Fe.

These two factors suggest that the entire plume near-field and bulge should be quite productive, especially north of the river mouth. Indeed, enhanced nutrient supply related to tidal-plume-induced mixing may be one factor causing the Washington shelf to exhibit higher primary productivity and standing Chl-a stock than the Oregon shelf, despite generally stronger upwelling off Oregon. However, Chl-a levels are often larger around the boundaries of the tidal plume than directly in a new ebb outflow – even if productivity is high, accumulation of sufficient standing stock to yield high Chl-a values takes some hours. Thus, a new ebb outflow may exhibit low Chl-a values even as nutrients are being mixed into it.

Ocean color images and other data that suggest that the outer part of the tidal plume and plume near-field are quite productive under upwelling, neutral and transitional conditions (e.g. Figs. 1-3, 9, and 10). Modest productivity is sometimes found even during downwelling. Examination of 56 ocean color images for 2004 to 2005 suggests, however, that productivity associated with the plume is not always on the west, northwest and north sides (e.g., Fig. 10). The mechanisms discussed here enhance productivity on the west, northwest and north sides of the plume during steady upwelling. Other parts of the plume near-field may experience enhanced mixing and productivity whenever the plume is strongly transient, especially in the offshore direction – as suggested by Fong and Geyer (2001), plume advection by shifting winds causes thinning of the plume and mixing.

This high productivity, and the vertical mixing on which it is based, occur despite high stratification. Indeed, the mixing induced by fronts and internal solitons is part of the "paradox of plume mixing" – mixing occurs through mechanisms (supercritical fronts and soliton generation) that exist only in a stratified environment. Furthermore, productivity is enhanced by the fact that the plume is the active layer in near-field mixing, so that entrainment into the tidal plume predominates, and the tidal plume maintains its identity for a sufficient length of time to allow photosysnthesis to take place in what is analogous to a shallow mixed layer. Locally, the strength of mixing or entrainment can be expressed in terms of a Richardson number – a ratio of buoyancy to stratification (e.g., Souza and Simpson, 1997). However, a parameterization of plume-related mixing (by both fronts and solitons) in terms of the bulk plume properties (e.g., river discharge, estuary mouth width and initial density difference) is lacking.

### 5.3. Salmonids and the Seasonality of Plume Processes

There is an important connection between the plume mixing processed discussed here and survival of the Pacific Northwest's endangered salmonids. Strong upwelling typically begins in late June (Hickey, 1989), and this timing has changed little over time. Though some out-migration occurred throughout the year, the largest number of juvenile salmonids also came downstream in late June and July (Bottom et al., 2005), just in time to utilize secondary productivity based on upwelled nutrients. Historically, this out-migration was associated with the spring freshet; now it is set by hatchery schedules.

A striking change has taken place in the Columbia River flow cycle over the last 125 years (Bottom et al., 2005), de-synchronizing it with the onset of upwelling and salmonid behavior. The peak river flow has shifted from late June prior to 1900 to late May. The freshet continues to migrate to earlier dates, because of an earlier snow melt and human alteration of the flow cycle. Moreover, the average and freshet peak flows have decreased ~15% and >40%, respectively, mostly due to human factors. Thus, before 1900, a large freshet peak typically occurred in late June about the same time as the onset of strong upwelling. This combination of high river flow and strong upwelling provided high levels of N, P, Si and micronutrients to the plume area and Oregon and Washington shelves. The frontal processes discussed here facilitated mixing of plume and upwelled nutrients. Moreover, colder water temperatures and the shorter residence time of water in the un-dammed, historical river likely caused the system to provide more nutrients to coastal waters than at present (Small et al., 1990). Thus, even if the largest historic freshets suppressed mixing for a time, productivity could have been supported by plume nutrients (cf. Fig. 2).

High levels of primary productivity (and the secondary production it supported) during and after the spring freshet must have provided seaward migrating juvenile salmonids with an ample food source. Also, the higher historic sediment load (at least double modern levels; Bottom et al., 2005) associated with larger historic freshets provided juvenile salmonids with protection from predation (Pearcy, 1992). While a full understanding of the support of salmonid survival by the coastal ecosystem remains elusive, the growing mismatch between the peak river flow (now late May) and the onset of upwelling and the peak of the juvenile salmonid migration (late June) may limit the ability of the coastal ocean to support juvenile salmonids.

## 6. Acknowledgement

This research was funded by the Bonneville Power Administration and NOAA-Fisheries (project: Ocean Survival of Salmonids), and the NSF (project RISE – River Influences on Shelf Ecosystems OCE 0239072). Thanks to Ed Dever of Oregon State University for current meter data. We also thank Captain Ron L. Short of the *R/V Pt Sur* and Marine Technicians Stewart Lamberdin, Christina Courcier, and Ben Jokinen for their superb support of in-situ data collection. The SAR images were provided by Comprehensive Large Array-data Stewardship System

(CLASS) of National Oceanic and Atmospheric Administration (NOAA). Thanks to Nate Mantua and Alan Hamlet of University of Washington for discussion of the connection between salmonid survival and freshet timing.

## 7. References


Barnes, C. A, C. Duxbury, and B.-A. Morse, 1972. Circulation and selected properties of the Columbia River plume at sea. In: A.T. Pruter and D.L. Alverson (Eds.), *The Columbia River Estuary and Adjacent Ocean Waters*, University of Washington Press, Seattle, pp. 41-80.

Bottom, D. L., C. A. Simenstad, J. Burke, A. M. Baptista, D. A. Jay, K. K. Jones, E. Casillas, M. H. Schiewe, 2005. *Salmon at river's end: The role of the estuary in the decline and recovery of Columbia River salmon.* U.S. Dept. of Commerce, NOAA Tech. Memo., NMFS-NWFSC-68, 246 pp.

Casillas, E., 1999. Role of the Columbia River estuary and plume in salmon productivity. In: *Ocean Conditions and the Management of Columbia River Salmon; Proceedings of a Symposium*, Portland, OR July 1, 1999, G. A. Bisbal (Ed.) Portland, OR: Northwest Power Planning Council, pp. 55-64.

Chao, S-Y, 1988. Wind-driven motion of estuarine plumes. *J. Phys. Oceanogr.,* 18:1144-1166.

Chao, S-Y, 1990. Tidal modulation of estuarine plumes. *J. Phys. Oceanogr.,* 20: 1115-1123.

Cudaback, C. N. and D. A. Jay, 1996. Buoyant plume formation at the mouth of the Columbia River – an example of internal hydraulic control? *Buoyancy Effects on Coastal and Estuarine Dynamics*, AGU Coastal and Estuarine Studies Volume 53:139-154.

Cudaback, C. N., and D. A. Jay, 2000. Tidal asymmetry in an estuarine pycnocline: 1, Depth and thickness. *J. Geophys. Res.,* 105: 26,237-26,252.

Fong, D.A. and W. R. Geyer, 2001. Response of a river plume during and upwelling favorable wind event. *J. Geophys. Res.,* 106:1067-1084.

Fong, D.A., W. R. Geyer, W.R., and R.P. Signell, 1997. The wind-forced response of a buoyant coastal current: Observations of the western Gulf of Maine plume. *J. Mar. Sys.*, 12:69-81.

Galbraith, P.S., and Kelley, D.E., 1996. Identifying overturns in CTD profiles. *J. Atmos. Ocean. Technol.,* 13:688-702.

Garcia-Berdeal, B.M. Hickey, and M. Kawase, 2002. Influence of wind stress and ambient flow on a high discharge river plume. *J Geophys. Res.,* 107: 3130 doi:1029/ 2001JC000392.

Garvine, R. W., 1982. A steady-state model for buoyant surface plume hydrodynamics in coastal waters. *Tellus,* 34:293-306.

Hickey, B.M., 1989. Patterns and processes of shelf and slope circulation. In *Coastal Oceanography of Washington and Oregon*, M. R. Landry and B. M. Hickey (Eds.), Elsevier Science, Amsterdam, pp. 41-115.

Hickey, B. M., L.J. Pietrafesa, D.A. Jay, and W.C. Boicourt, 1998. The Columbia River Plume Study – Subtidal Variability in the Velocity and Salinity Fields. *J. Geophys. Res.,* 103:10339-10368.

Hickey, B. M., Geier, S. L., Kachel, N. B., & MacFadyen, A., 2005. A bi-directional river plume: The Columbia in summer. *Contin. Shelf Res.*, 25:1631-1656

Horner-Devine, A.R., D.A. Fong, S.G. Monismith and T. Maxworthy, 2006. Laboratory experiments simulating a coastal river discharge. *J. Fluid Mech.,* 555:203-232.

Horner-Devine, A. R., D. A. Jay, P. M. Orton, and E. Spahn, 2007. A plume within a plume: a conceptual model of the strongly tidal Columbia plume, submitted to *J. Mar. Sys.* (this volume).

Jay, D. A., P. M. Orton, and T. Chisholm, 2002. Speculations on Human and Climate-Change Alteration of Iron Input to Upwelling Areas off Oregon and Washington, Eastern Pacific Ocean Conference, Timberline Lodge, OR, September 2002.

Kay, D.J., and D.A. Jay, 2003. Interfacial mixing in a highly stratified estuary 1: Characteristics of mixing. *J. Geophys. Res.,* 108 3072, doi:10.1029/2000JC000252.

Landry, M.R., J.R. Postel, W.K. Peterson and J. Newman, 1989. Broad-scale distributional patterns of hydrographic variables on the Washington/Oregon shelf. In *Coastal Oceanography of Washington and Oregon*, M. Landry and B. M. Hickey (Eds.), Elsevier, Amsterdam, pp. 1-40.

Lohan, M.C. and K.W. Bruland, 2006. The importance of vertical mixing for the supply of nitrate and iron to the Columbia River plume: implications for biology. Submitted to *Mar. Chem*.

Macdonald, D.G. and Geyer, W.R., 2004. Turbulent Energy Production and Entrainment at a Highly Stratified Estuarine Front. *J. Geophys. Res.,* 109 C05004, doi:10.1029/ 2003JC002094.

Nash, J. D., Moum, J. N., 2005. River plumes as a source of large-amplitude internal waves in the coastal ocean. *Nature,* 43: 400-403

O'Donnell, J., G. O. Marmorino and C.L. Trump, 1998. Convergence and downwelling at a river plume front. *J. Phys. Oceanogr.,* 28, 1481-1495.

O'Donnell, J., S. G. Ackleson and E. R. Levine, 2006. Convergence and downwelling at a river plume front. Submitted to *J. Geophys. Res.*

Orton, P. M., and D. A. Jay, 2005. Observations at the tidal plume front of a high-volume river outflow. *Geophys. Res. Lett.*, 32, L11605, doi:10.1029/2005GL022372.

Ott, M.W., J.A. Barth, and A.Y. Erofeev, 2004. Microstructure measurements from a towed undulating platform. *J. Atmos. Oceanic Technol.*, 21, 1621-1632.

Pan, J., D A. Jay, and P M. Orton, 2006. Analyses of Internal Solitary Waves Generated by the Columbia River Plume. Submitted to *J. Geophys. Res.*

Pan, J. and D. A. Jay, 2006. Vertical Mixing and Horizontal Transport Caused by Large Amplitude Internal Solitons in the Columbia River Plume Region, Physics of Estuaries and Coastal Seas 2006, Astoria, OR, September 2006.

Pearcy, W.G. 1992. *Ocean Ecology of North Pacific Salmon*, Washington Sea Grant Program, University of Washington Press, Seattle, WA, 179 pp.

Peters, H., and Johns, W.E., 2004. Mixing and entrainment in the Red Sea outflow plume. II. Turbulence characteristics. *J. Phys. Oceanogr*, in press.

Seim, H.E. and Gregg, M.C., 1994. Detailed observations of a naturally occurring shear instability. *J. Geophys. Res.,* 99: 10049-10073.

Small, L. F., C. D. McIntire, K.B. Macdonald, J. R. Lara-Lara, B.E. Frey, M. C. Amspoker and T. Winfield, 1990. Primary production, plant and detrital biomass, and particle transport in the Columbia River Estuary. *Progr. Oceanogr.,* 25: 175-210.

Souza, A. J., and J. H. Simpson, 1997. Controls on stratification in the Rhine ROFI system. *J. Mar. Sys.,* 12: 311-323.

Thomas, A. C., and R. A. Weatherbee, 2005. Satellite-measured temporal variability of the Columbia River plume. *Rem. Sens. Environ.* 100: 167-178.

Thorpe, S.A., 1977. Turbulence and mixing in a Scottish loch. *Philos. Trans. R. Soc. London A*, 286:125-181.

Yankovsky, A.E., and D.C. Chapman, 1997. A simple theory for the fate of buoyant coastal discharges. *J. Phys. Oceanogr.,* 27, 1386-1401.

**Figure Captions**

***Figure 1:*** The Columbia River plume and its influence shown in (a) by SPM and (b) by Chl-a; MODIS derived images for 12 July 2004 at 2130, 5 hrs after high water (lesser ebb, two days after a neap). Weak upwelling-favorable winds prevailed. River flow during the week prior to these images averaged ~5,000 $m^3s^{-1}$, well below average for July. In (b), the circular plume bulge area of high productivity near the river mouth probably contains the water from several ebbs. High Chl-a levels are also seen along the coast, north and south of the river mouth. The bulk plume, as indicated by the SPM distribution trends southward and offshore; this is most evident in the SPM distribution.

***Figure 2***: Transition to upwelling: a map obtained 29 May to 3 June 2005 of salinity and Chl-a ~3 m below free surface during RISE-2; data are from the *R/V Pt. Sur* UDAS. Plume waters have moved southwestward under the influence of weak upwelling-favorable winds, but old plume waters remain at the surface along the coast except at the very south end of the map. The large volume of freshwater input by the spring freshet caps upwelled waters along the coast; elevated Chl-a levels are seen only within the plume. Several storms during May caused nutrient levels in river water to be above average for the season.

***Figure 3:*** Moderate downwelling winds: a map obtained 18-20 June 2005 of salinity and Chl-a ~3 m below free surface during RISE-2; data are from the *R/V Pt. Sur* flow-through system. Low salinity, new plume water is found only in the near-field and north of the river mouth, though old plume water is found to the south. Downwelling-favorable winds had reached 10 $ms^{-1}$ on 17 June, but winds dropped to light and variable by the end of the survey period.

***Figure 4:*** Moderate downwelling winds: a MODIS-derived Chl-a for 18 June 2004; Chl-a standing stock is generally low and mostly associated with plume waters.

***Figure 5:*** Conceptual sketch (from Horner et al., this volume) of the plume showing: (1) the plume source zone, (2) the tidal plume or plume near-field, (3) the plume bulge, and (4) the plume far-field, all in response to different forcing. Scenarios are: without wind forcing in a),

with downwelling winds in b), and with upwelling in c). Large arrows show the wind direction. The configuration for weak summer downwelling is a hybrid of a) and b).

***Figure 6:*** Hypothetical vorticity incurred by the upwind plume front for (a) upwelling and (b) downwelling. Vorticity in (a) is shown on a background of a SAR image for 26 July 2004 at 1439 UT, 8 hrs after high water (a greater ebb, moderate tidal range). Vorticity in (b) is shown on a background of a SAR image for 24 May 2003 at 1439 UT, ~10 hrs after high water (neap tide). In (a), the tidal plume front is still intact along the upwind (north) side of the plume. Internal wave generation began on the south and southwest sides of the front and has progressed around to the northwest side; the point of fission is indicated. There are 10-12 solitons visible on the west side of the plume. In (b) the upwind south/ southwest quadrant of the tidal plume front has dissipated. Internal waves south of the river mouth, both inside and outside the tidal plume, appear to have originated in deep water and are propagating landward. The location of the moored data in Fig. 8 is shown by "X" in (a).

***Figure 7:*** A north-south section across the plume along 124.33º W; from Horner-Devine et al. this volume), taken 9 June 2005 starting at 0222, ~3 hrs after high water on a lesser ebb (moderate tides with a strong diurnal inequality); river flow varied from 7,800 to 9,200 $m^3s^{-1}$ over the previous week. Shown are: in (a) a salinity section, (b) an east-west velocity section, (c) surface velocity components, and (d) surface velocity vectors and location; from Horner-Devine et al. (2007, this volume).

***Figure 8***: 300 kHz ADCP current meter and wind times series for July 2004 for the central RISE mooring at 46 10.02º N 124 11.72º W, in 69 m water depth. The data, plotted as stick vectors, were provided by Edward Dever, Oregon State University. Current data have been low-passed to remove tides; wind data have been filtered to remove diurnal sea breeze effects. From top to bottom: wind, currents at 1.5 m, currents at 25 m, and depth averaged velocity, all in $ms^{-1}$. Time on the x-axis is in calendar days, July 2004 (PST). See Fig. 6a for mooring location.

***Figure 9:*** Well-established upwelling: a map obtained 24-27 July 2004 of salinity (left) and Chl-a (right) at ~ 2 m depth during RISE-1. Data are from the R/V Pt UDAS; tides were weak. Plume

waters have moved southward under the influence of sustained upwelling favorable winds. Upwelled waters are seen shoreward of the plume.

***Figure 10:*** MODIS-derived Chl-a for 23 July 2004 at 2110 UT, ~ 8 hrs after high water (neap tide); Chl-a standing stock is generally low and mostly associated with plume waters.

***Figure 11:*** Section showing soliton fission from a northwestern plume front on 13 June 2005 1638 to 1941 UT; frontal crossing occurred at ~1810 UT, ~5.6 hrs after high water (neap tide). Shown are: a) salinity (b) cross-frontal velocity in $ms^{-1}$ from the 1200 kHz ADCP, c) ADCP acoustic backscatter, and (d) a detail from the acoustic backscatter section; note the difference in the horizontal scale in (d). The acoustic image provides a higher resolution than the TRIAXUS salinity data. Turbulence parameters for this section are shown in Fig. 13.

***Figure 12:*** Detail of soliton movement away from the northwestern plume front. Shown are: a) salinity, b) cross-frontal velocity in $ms^{-1}$ from the 1200 kHz ADCP, and c) ADCP acoustic backscatter. Data were collected during a 3-hour transect staring 13 June 2005 at 1947 UT; frontal crossing occurred at ~2100 UT, ~8 hrs after high water (neap tide). This captures a later stage in evolution of the soliton train than Fig. 11.

***Figure 13****:* A mixing summary diagram for the section shown in Fig. 11 (but extending further in the seaward direction), crossing the front at ~5.6 hrs after high water (neap tide). Shown in (a) is density, with superimposed overturn patches as rectangles. The left side of the rectangle marks the location of the patch in terms of the x-axis. The height of the patch represents the height for the patch, following the depth scale to the left. The width of the patch represents the Thorpe scale for the patch, also following the depth scale. Shown in (b) is transect location and in (c), floor and ceiling values for transect-mean eddy diffusivity (red) and turbulent kinetic energy dissipation (blue), both bin-averaged over the transect in terms of density.

***Figure 14:*** SAR image taken 19 July 2004 at 1428 UT, about 5.5 hrs after high water under downwelling conditions (2 d after a spring tide), simultaneous with a TRIAXUS section. The Pt Sur UDAS salinity data overlaid on the SAR image were collected between 1322 and 1511 UT.

The southern front is diffuse and deeper than upwelling fronts. There has been a transition between the time of the two transects from supercritical to subcritical conditions.

***Figure 15:*** Downwelling conditions: a TRIAXUS section corresponding to the first, more landward transect in Fig. 15; data were collected 19 July 2004, 4-5 hours after high water (2 d after a spring tide). Shown are: (a) Triaxus salinity, and (b) across-frontal velocity as a function of depth, with the frontal internal Froude number $F_R$. $F_R$ is calculated for the front relative to upstream conditions using the zones shown in (b). The entire frontal zone is, however, somewhat wider, extending from ~46.166 to 46.172º N, >300 m.

***Figure 16:*** Downwelling conditions: a TRIAXUS section corresponding to the second, more seaward transect in Fig. 15; data were collected 19 July 2004, 5-6 hours after high water (2 d after a spring tide). Shown are: (a) Triaxus salinity, and (b) across-frontal velocity as a function of depth, with the frontal internal Froude number $F_R$. $F_R$ is calculated for the front relative to upstream conditions as indicated in (b). A transition from critical to sub-critical conditions has occurred between the two sections. $F_R$ is calculated for the front relative to upstream conditions using the zones shown in (b). The entire frontal zone is broad, extending from ~46.167 to 46.2º N, >2 km.

***Figure 17:*** A SAR image taken under upwelling conditions on 9 August 2002, ~6.5 hours after high water on a spring tide; the river flow was 4,700 $m^3s^{-1}$. Internal waves generated both by the plume and over the slope are seen.

***Figure 18:*** A SAR image taken under downwelling conditions on 26 May 2002, ~6 hrs after high water (greater ebb, spring tide). Internal wave generation begins from the south side of the plume, just as under upwelling conditions.

(a) (b)

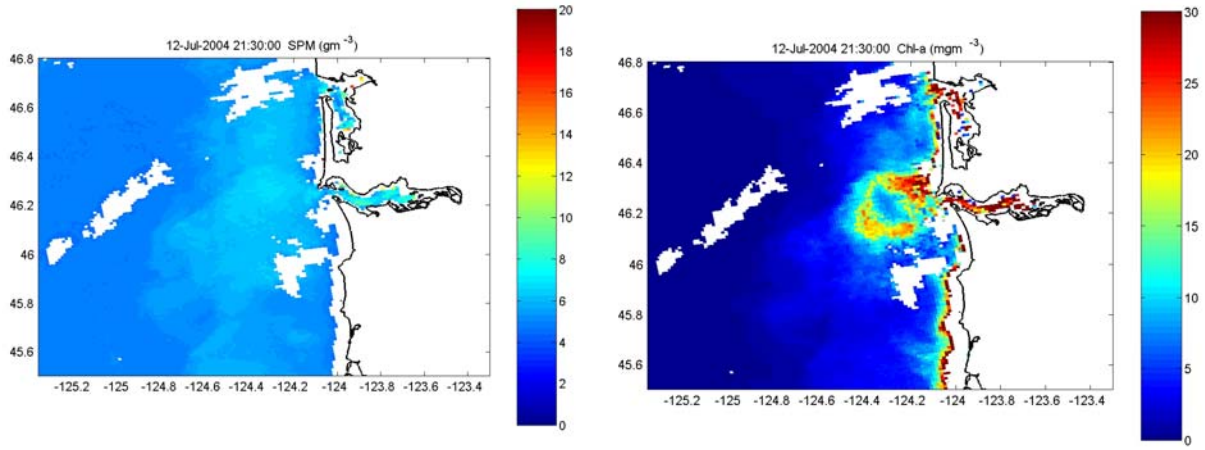


***Figure 1:*** The Columbia River plume and its influence shown in (a) by SPM and (b) by Chl-a; MODIS derived images for 12 July 2004 at 2130, 5 hrs after high water (lesser ebb, two days after a neap). Weak upwelling-favorable winds prevailed. River flow during the week prior to these images averaged ~5,000 $m^3s^{-1}$, well below average for July. In (b), the circular plume bulge area of high productivity near the river mouth probably contains the water from several ebbs. High Chl-a levels are also seen along the coast, north and south of the river mouth. The bulk plume, as indicated by the SPM distribution trends southward and offshore; this is most evident in the SPM distribution.

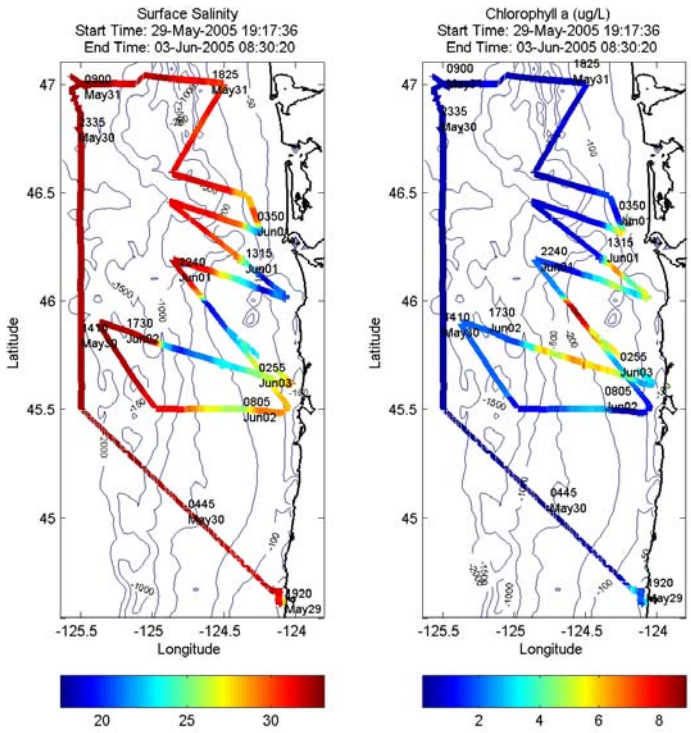


***Figure 2***: Transition to upwelling: a map obtained 29 May to 3 June 2005 of salinity and Chl-a ~3 m below free surface during RISE-2; data are from the *R/V Pt. Sur* UDAS. Plume waters have moved southwestward under the influence of weak upwelling-favorable winds, but old plume waters remain at the surface along the coast except at the very south end of the map. The large volume of freshwater input by the spring freshet caps upwelled waters along the coast; elevated Chl-a levels are seen only within the plume. Several storms during May caused nutrient levels in river water to be above average for the season.

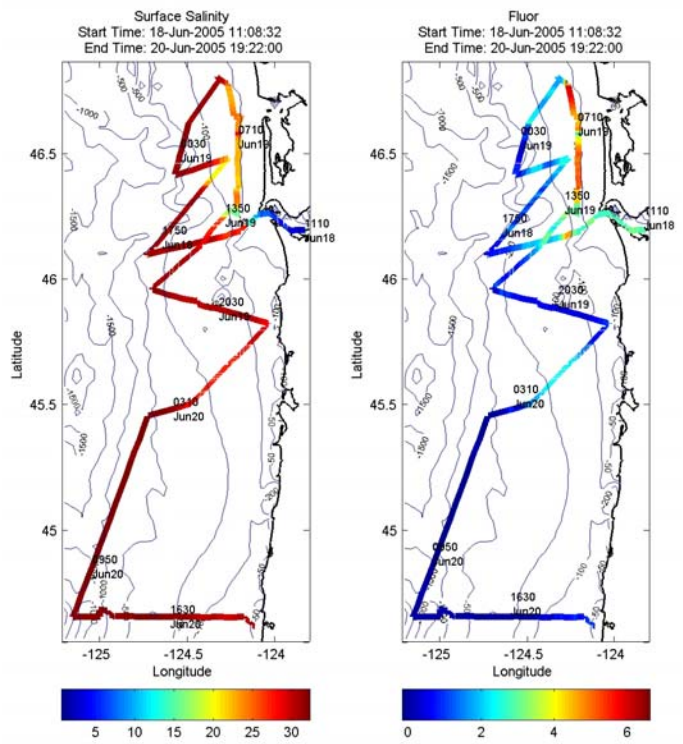


***Figure 3:*** Moderate downwelling winds: a map obtained 18-20 June 2005 of salinity and Chl-a ~3 m below free surface during RISE-2; data are from the *R/V Pt. Sur* flow-through system. Low salinity, new plume water is found only in the near-field and north of the river mouth, though old plume water is found to the south. Downwelling-favorable winds had reached 10 $ms^{-1}$ on 17 June, but winds dropped to light and variable by the end of the survey period.

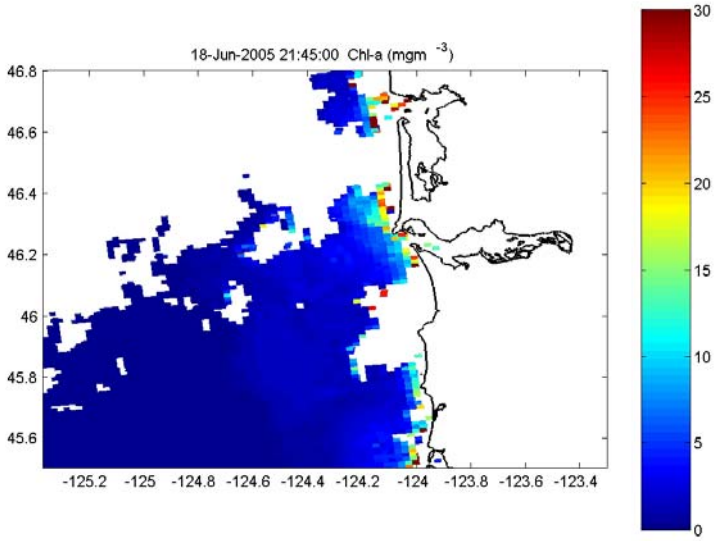


***Figure 4:*** Moderate downwelling winds: a MODIS-derived Chl-a for 18 June 2004; Chl-a standing stock is generally low and mostly associated with plume waters.

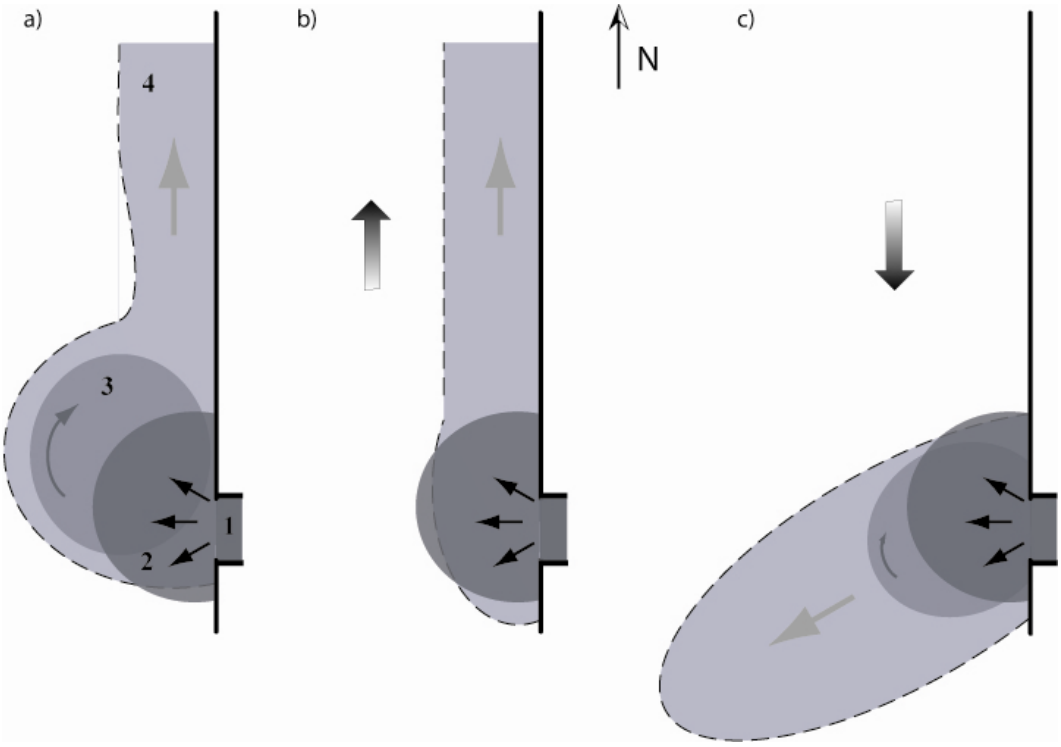


***Figure 5:*** Conceptual sketch (from Horner et al., this volume) of the plume showing: (1) the plume source zone, (2) the tidal plume or plume near-field, (3) the plume bulge, and (4) the plume far-field, all in response to different forcing. Scenarios are: without wind forcing in a), with downwelling winds in b), and with upwelling in c). Large arrows show the wind direction. The configuration for weak summer downwelling is a hybrid of a) and b).

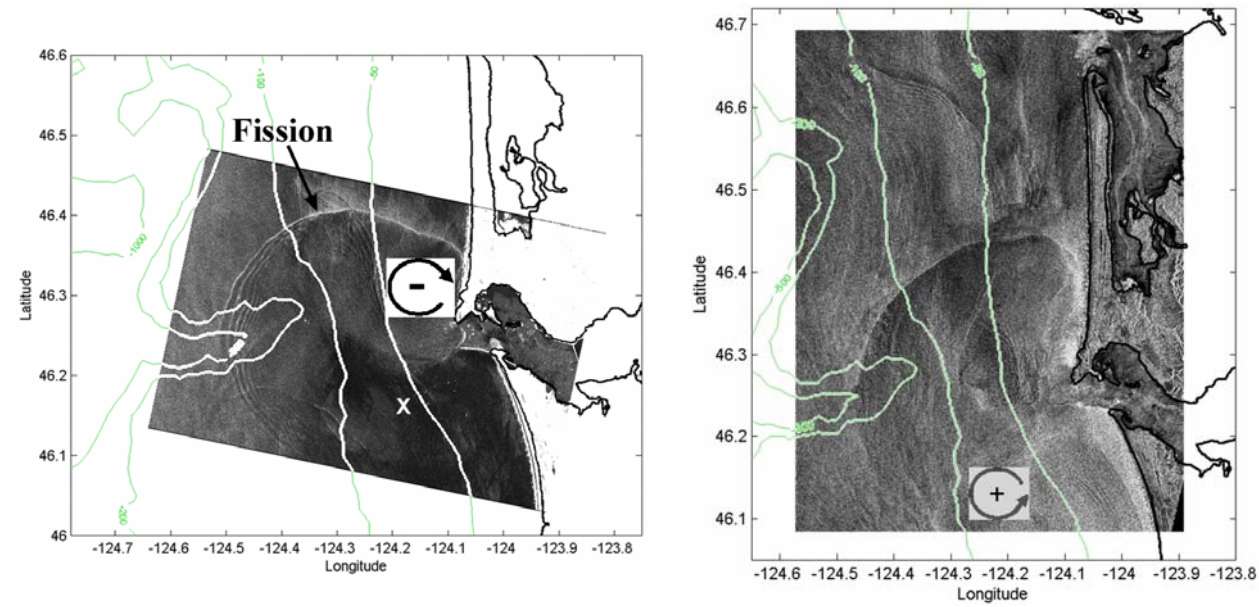


(a) (b)

***Figure 6:*** Hypothetical vorticity incurred by the upwind plume front for (a) upwelling and (b) downwelling. Vorticity in (a) is shown on a background of a SAR image for 26 July 2004 at 1439 UT, 8 hrs after high water (a greater ebb, moderate tidal range). Vorticity in (b) is shown on a background of a SAR image for 24 May 2003 at 1439 UT, ~10 hrs after high water (neap tide). In (a), the tidal plume front is still intact along the upwind (north) side of the plume. Internal wave generation began on the south and southwest sides of the front and has progressed around to the northwest side; the point of fission is indicated. There are 10-12 solitons visible on the west side of the plume. In (b) the upwind south/ southwest quadrant of the tidal plume front has dissipated. Internal waves south of the river mouth, both inside and outside the tidal plume, appear to have originated in deep water and are propagating landward. The location of the mooring data in Fig. 8 is shown by "X" in (a).

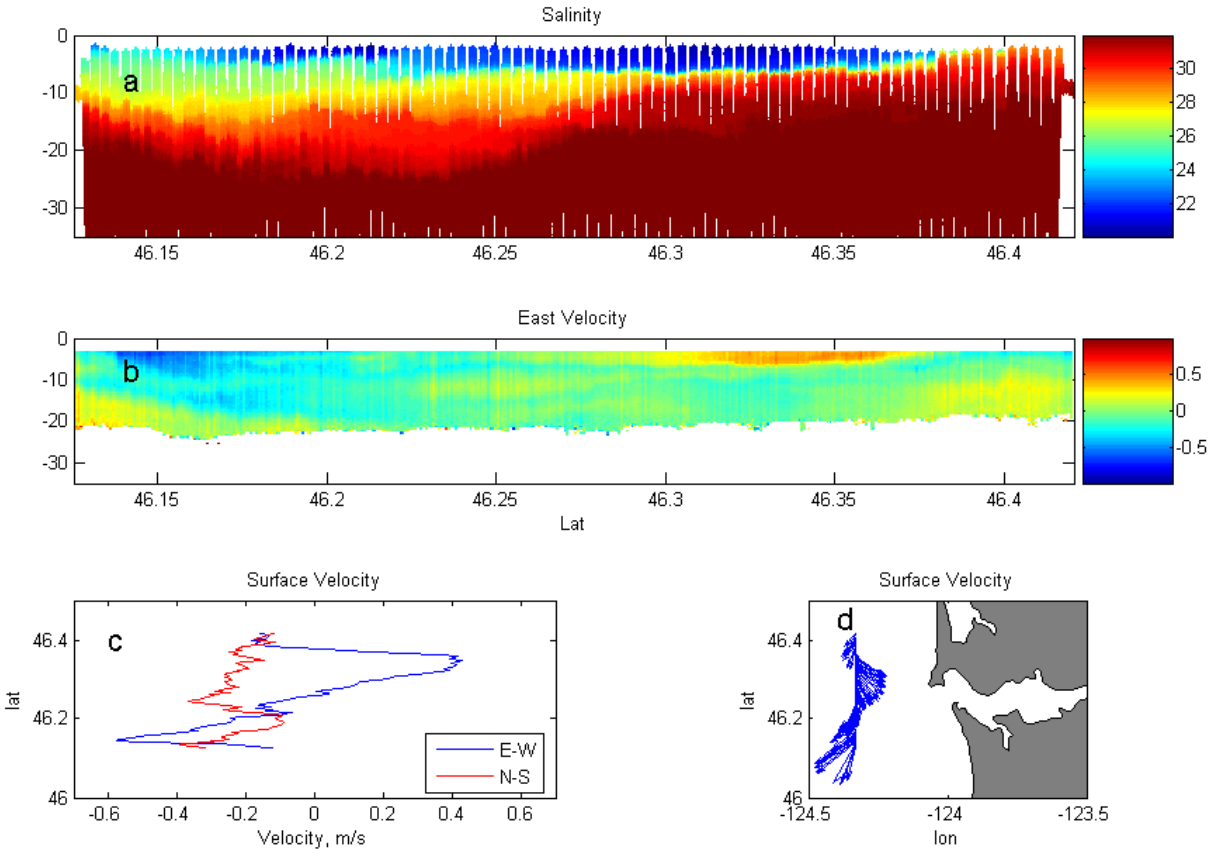


***Figure 7:*** A north-south section across the plume along 124.33º W; from Horner-Devine et al. this volume), taken 9 June 2005 starting at 0222, ~3 hrs after high water on a lesser ebb (moderate tides with a strong diurnal inequality); river flow varied from 7,800 to 9,200 $m^3s^{-1}$ over the previous week. Shown are: in (a) a salinity section, (b) an east-west velocity section, (c) surface velocity components, and (d) surface velocity vectors and location.

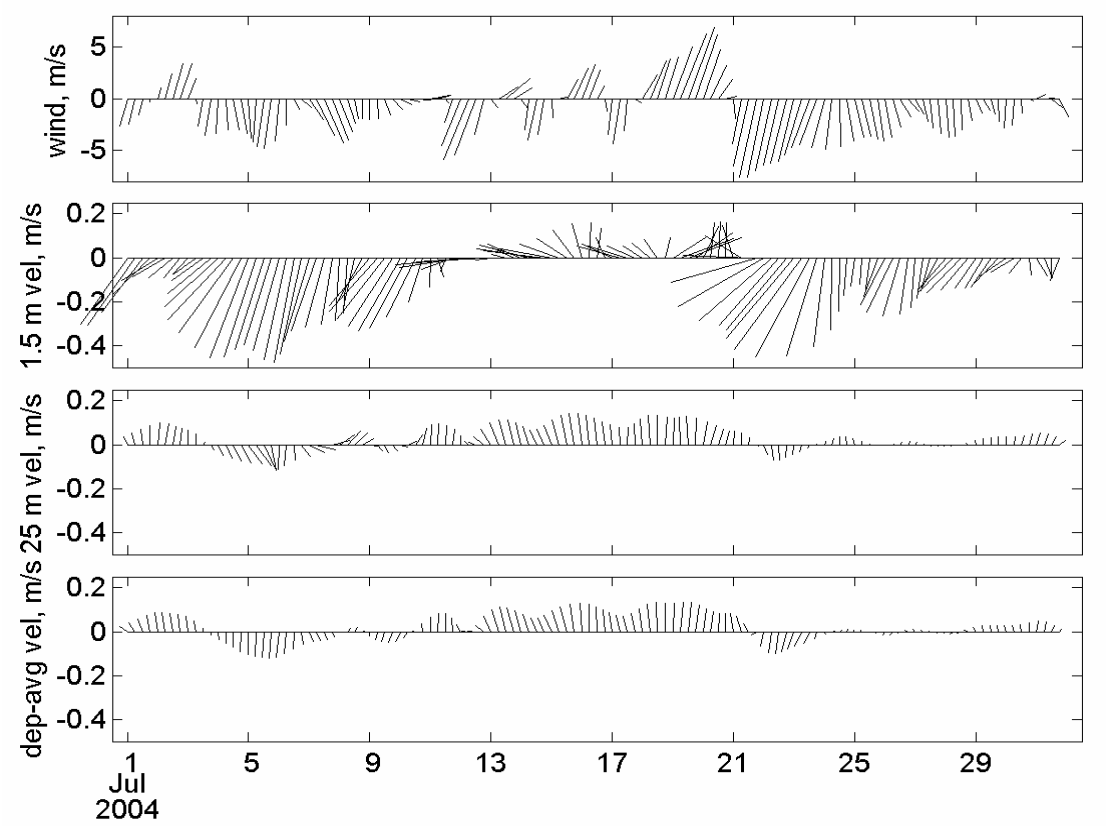


***Figure 8***: 300 kHz ADCP current meter and wind times series for July 2004 for the central RISE mooring at 46 10.02º N 124 11.72º W, in 69 m water depth. The data, plotted as stick vectors, were provided by Edward Dever, Oregon State University. Current data have been low-passed to remove tides; wind data have been filtered to remove diurnal sea breeze effects. From top to bottom: wind, currents at 1.5 m, currents at 25 m, and depth averaged velocity, all in $ms^{-1}$. Time on the x-axis is in calendar days, July 2004 (PST). See Fig. 6a for mooring location.

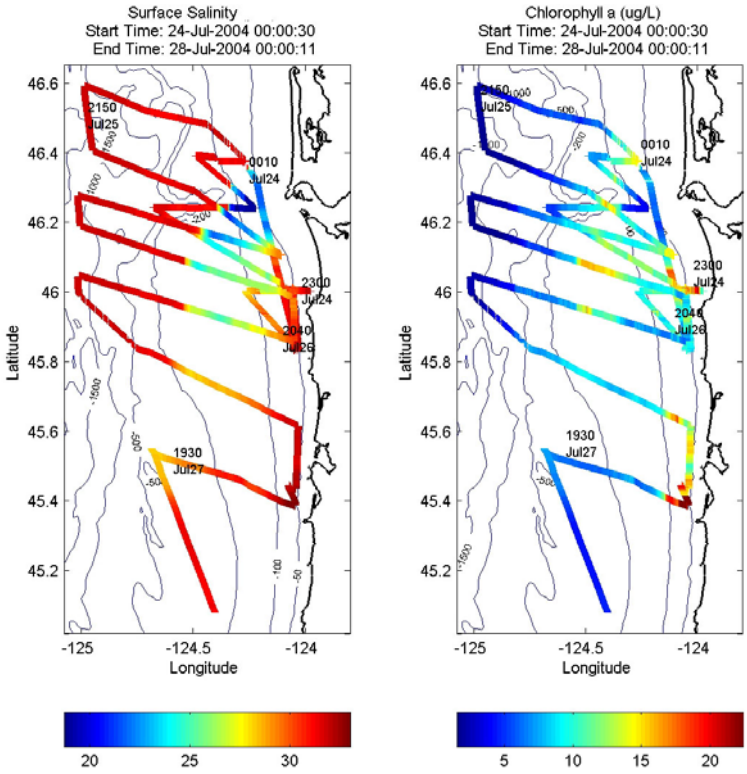


***Figure 9:*** Well-established upwelling: a map obtained 24-27 July 2004 of salinity (left) and Chl-a (right) at ~ 2 m depth during RISE-1. Data are from the R/V Pt UDAS; tides were weak. Plume waters have moved southward under the influence of sustained upwelling favorable winds. Upwelled waters are seen shoreward of the plume, and old plume water is seen on the seaward side of the at about 45.6º N, -124.7º W. this water had been located along the coast north of the river mouth before upwelling began on 20 July 2004.

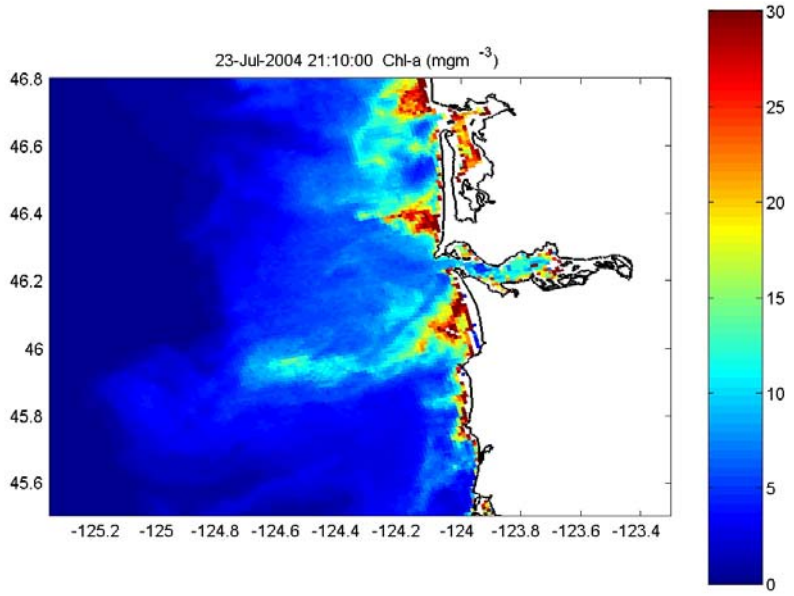


***Figure 10:*** MODIS-derived Chl-a for 23 July 2004 at 2110 UT, ~ 8 hrs after high water (neap tide); Chl-a standing stock is generally low and mostly associated with plume waters.

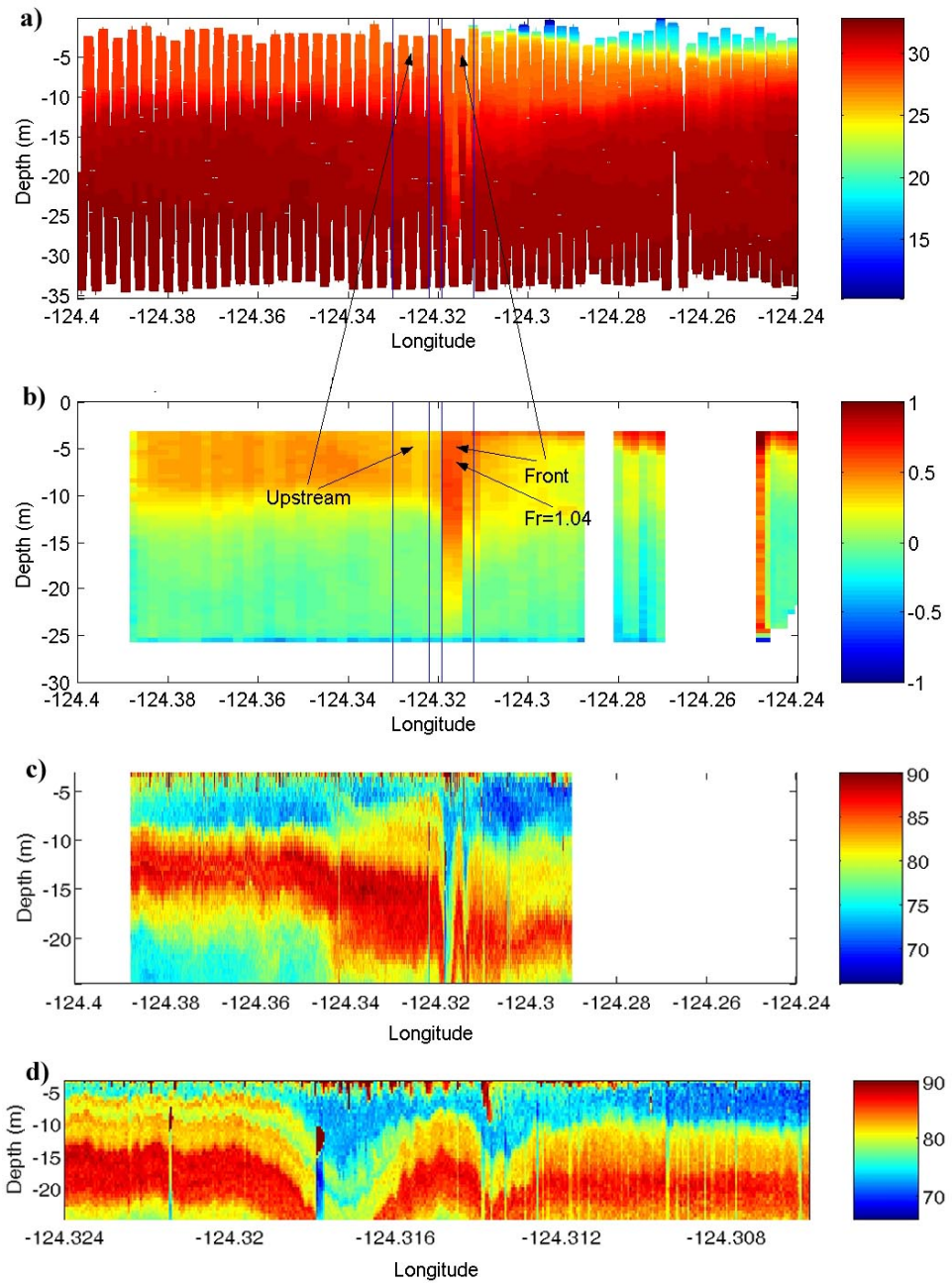


***Figure 11:*** Section showing soliton fission from a northwestern plume front on 13 June 2005 1638 to 1941 UT; frontal crossing occurred at ~1810 UT, ~5.6 hrs after high water (neap tide). Shown are: a) salinity (b) cross-frontal velocity in $ms^{-1}$ from the 1200 kHz ADCP, c) ADCP acoustic backscatter, and (d) a detail from the acoustic backscatter section; note the difference in the horizontal scale in (d). The acoustic image provides a higher resolution than the TRIAXUS salinity data. Turbulence parameters for this section are shown in Fig. 13.

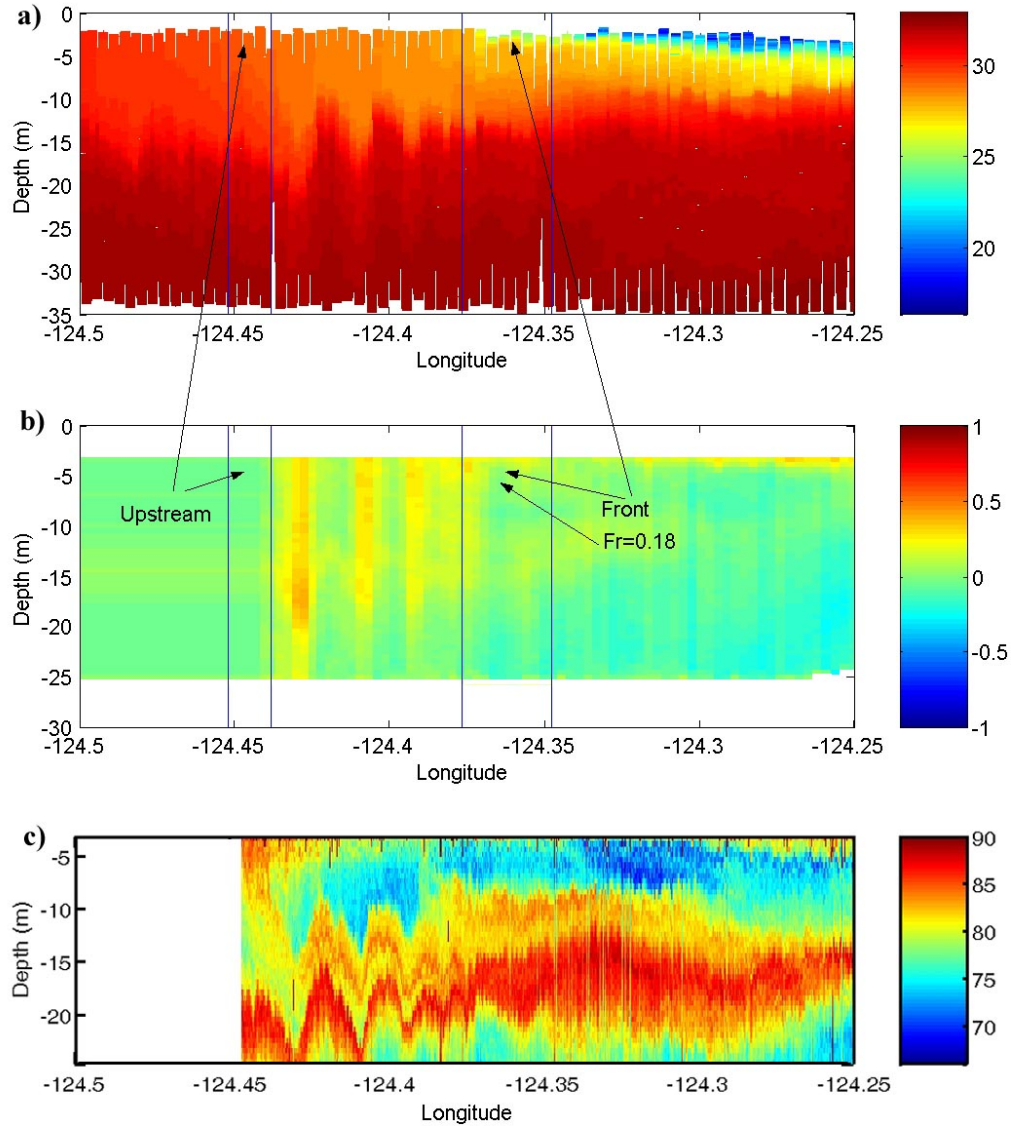


***Figure 12:*** Detail of soliton movement away from the northwestern plume front. Shown are: a) salinity, b) cross-frontal velocity in $ms^{-1}$ from the 1200 kHz ADCP, and c) ADCP acoustic back-scatter. Data were collected during a 3-hour transect staring 13 June 2005 at 1947 UT; frontal crossing occurred at ~2100 UT, ~8 hrs after high water (neap tide). This captures a later stage in evolution of the soliton train than Fig. 11.

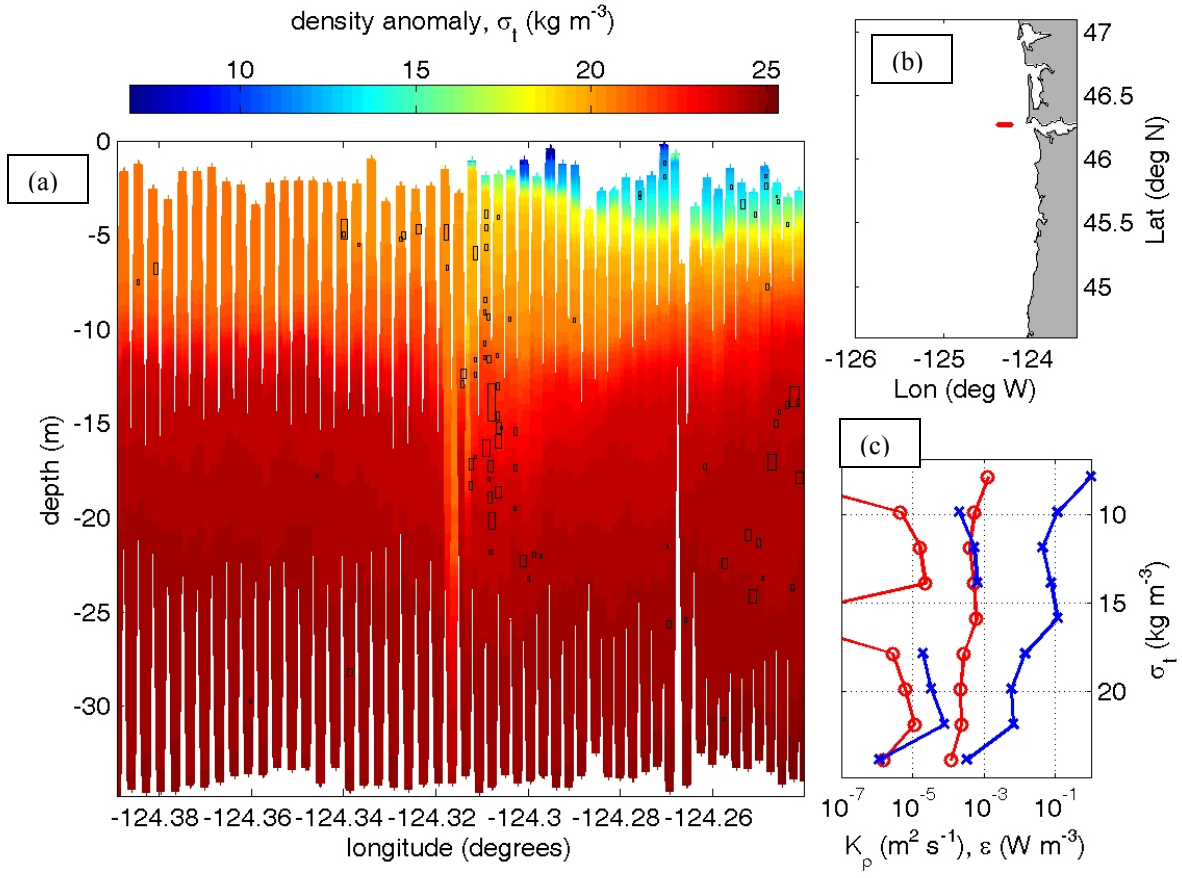


***Figure 13****:* A mixing summary diagram for the section shown in Fig. 11 (but extending further in the seaward direction), crossing the front at ~5.6 hrs after high water (neap tide). Shown in (a) is density, with superimposed overturn patches as rectangles. The left side of the rectangle marks the location of the patch in terms of the x-axis. The height of the patch represents the height for the patch, following the depth scale to the left. The width of the patch represents the Thorpe scale for the patch, also following the depth scale. Shown in (b) is transect location and in (c), floor and ceiling values for transect-mean eddy diffusivity (red) and turbulent kinetic energy dissipation (blue), both bin-averaged over the transect in terms of density.

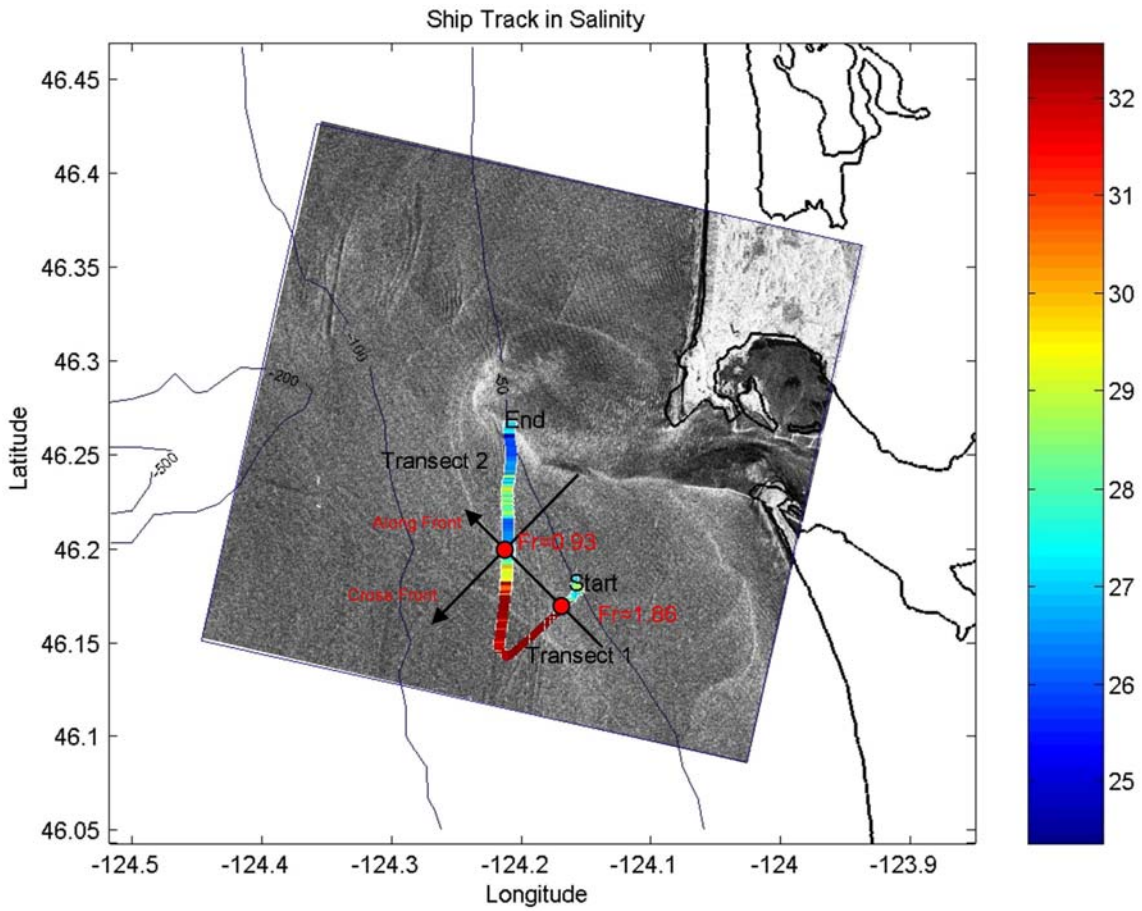


***Figure 14:*** SAR image taken 19 July 2004 at 1428 UT, about 5.5 hrs after high water under downwelling conditions (2 d after a spring tide), simultaneous with a TRIAXUS section. The Pt Sur UDAS salinity data overlaid on the SAR image were collected between 1322 and 1511 UT. The southern front is diffuse and deeper than upwelling fronts. There has been a transition between the time of the two transects from supercritical to subcritical conditions.

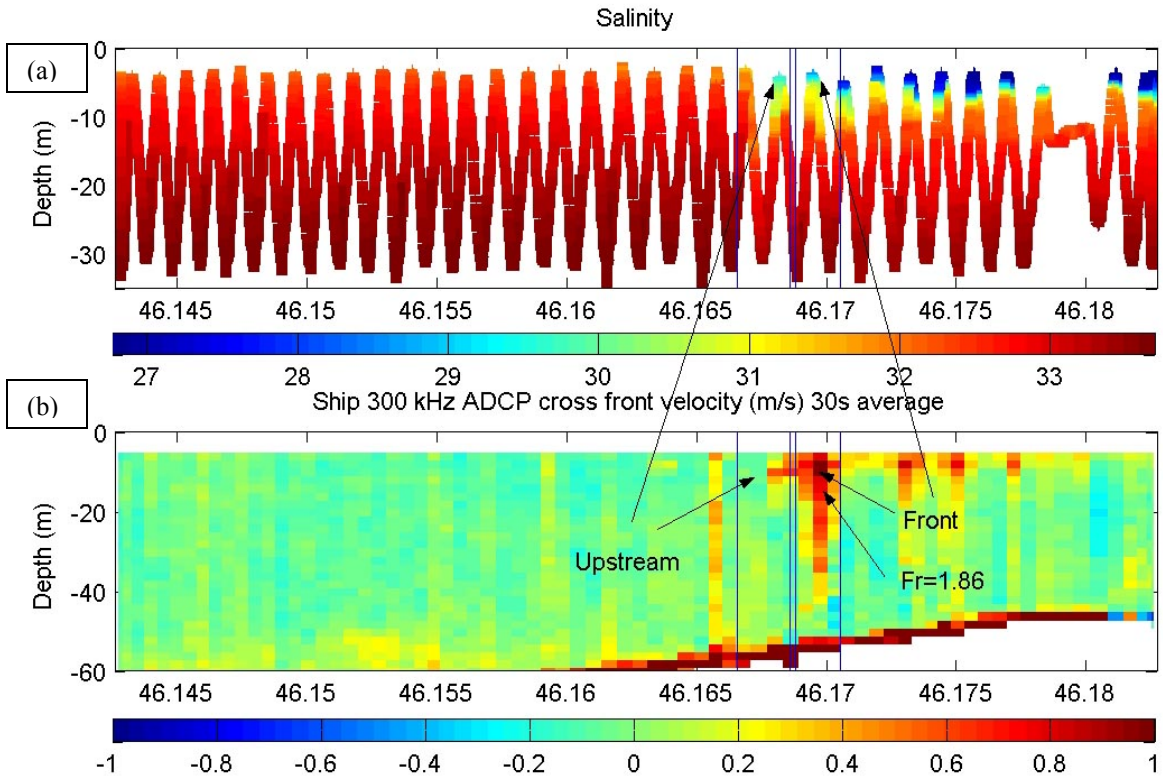


***Figure 15:*** Downwelling conditions: a TRIAXUS section corresponding to the first, more landward transect in Fig. 15; data were collected 19 July 2004, 4-5 hours after high water (2 d after a spring tide). Shown are: (a) Triaxus salinity, and (b) across-frontal velocity as a function of depth, with the frontal internal Froude number $F_R$. $F_R$ is calculated for the front relative to upstream conditions using the zones shown in (b). The entire frontal zone is, however, somewhat wider, extending from ~46.166 to 46.172º N, >300 m.

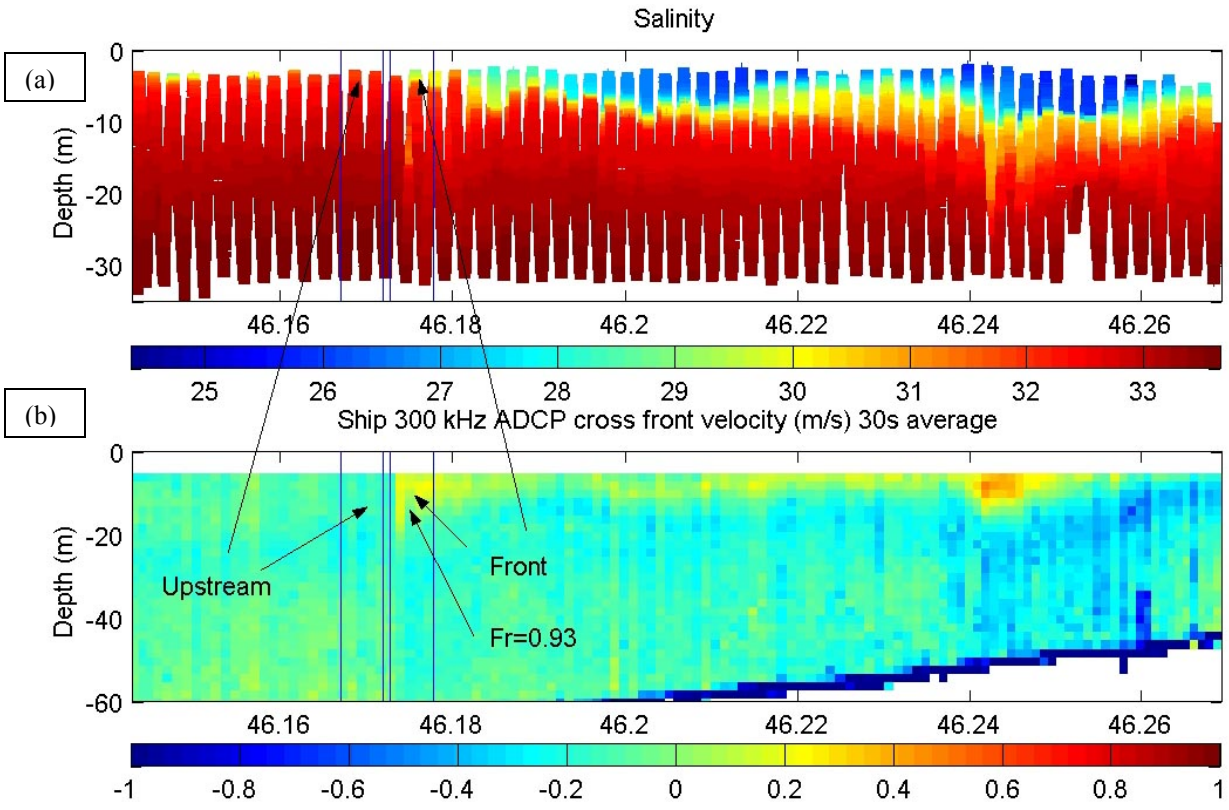


***Figure 16:*** Downwelling conditions: a TRIAXUS section corresponding to the second, more seaward transect in Fig. 15; data were collected 19 July 2004, 5-6 hours after high water (2 d after a spring tide). Shown are: (a) Triaxus salinity, and (b) across-frontal velocity as a function of depth, with the frontal internal Froude number $F_R$. $F_R$ is calculated for the front relative to upstream conditions as indicated in (b). A transition from critical to sub-critical conditions has occurred between the two sections. $F_R$ is calculated for the front relative to upstream conditions using the zones shown in (b). The entire frontal zone is broad, extending from ~46.167 to 46.2º N, >2 km.

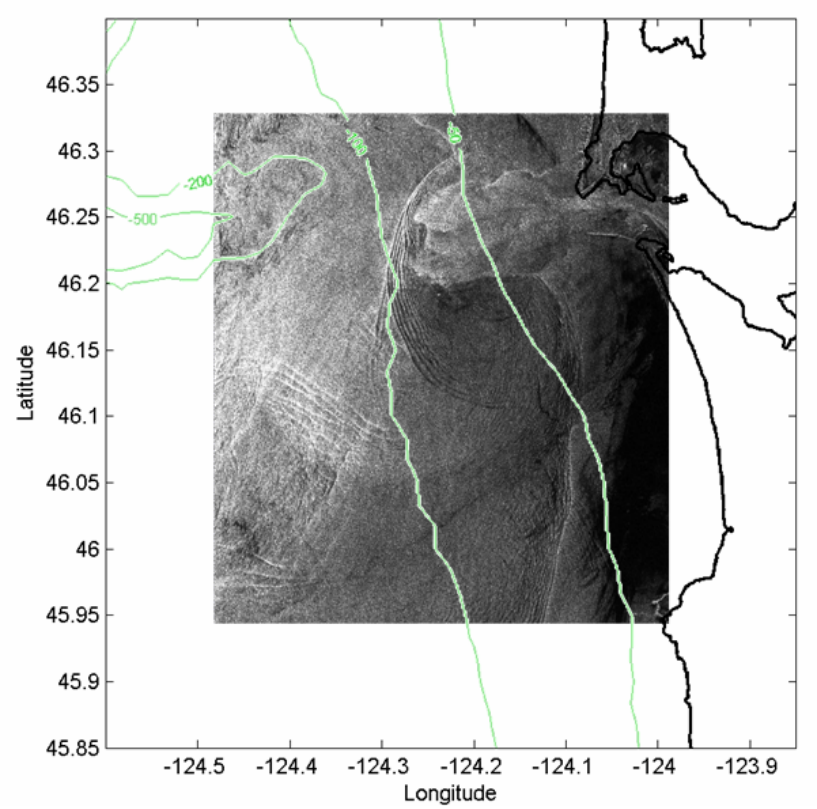


***Figure 17:*** A SAR image taken under upwelling conditions on 9 August 2002, ~6.5 hours after high water on a spring tide; the river flow was 4,700 $m^3s^{-1}$. Internal waves generated both by the plume and over the slope are seen.

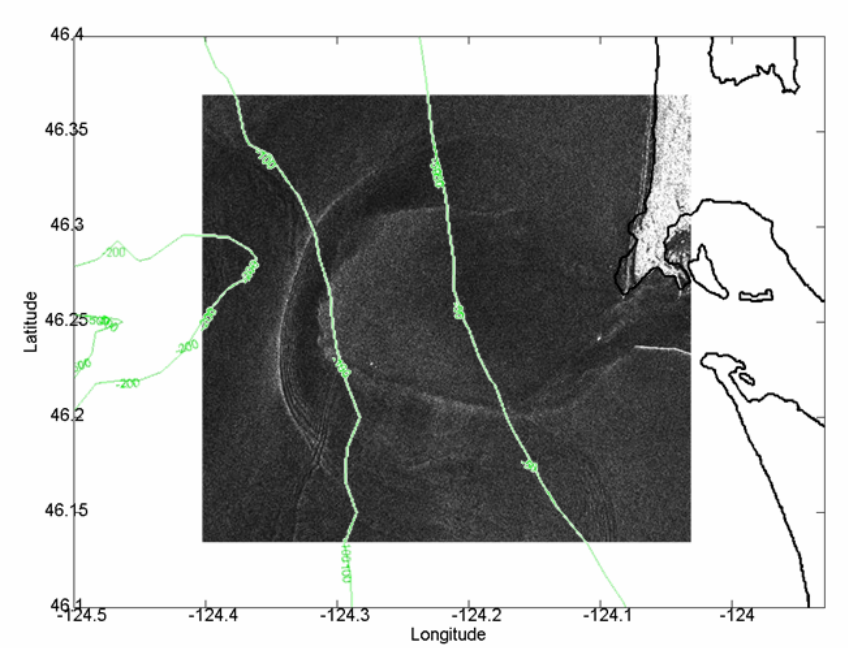


***Figure 18:*** A SAR image taken under downwelling conditions on 26 May 2002, ~6 hrs after high water (greater ebb, spring tide). Internal wave generation begins from the south side of the plume, just as under upwelling conditions.